Conditional Hyperbolic Quadrature Method of Moments for Kinetic Equations

Rodney O Fox, Frédérique Laurent, Aymeric Vié

▶ **To cite this version:**

Rodney O Fox, Frédérique Laurent, Aymeric Vié. Conditional Hyperbolic Quadrature Method of Moments for Kinetic Equations. Journal of Computational Physics, 2018, 365, pp.269–293. hal-01632813v1

HAL Id: hal-01632813

https://hal.science/hal-01632813v1

Submitted on 10 Nov 2017 (v1), last revised 6 Apr 2018 (v2)

HAL is a multi-disciplinary open access archive for the deposit and dissemination of scientific research documents, whether they are published or not. The documents may come from teaching and research institutions in France or abroad, or from public or private research centers.

L'archive ouverte pluridisciplinaire **HAL**, est destinée au dépôt et à la diffusion de documents scientifiques de niveau recherche, publiés ou non, émanant des établissements d'enseignement et de recherche français ou étrangers, des laboratoires publics ou privés.

Conditional Hyperbolic Quadrature Method of Moments for Kinetic Equations

Rodney O. Fox[a,b,c], Frédérique Laurent[b,c], Aymeric Vié[b,c]

[a] *Department of Chemical and Biological Engineering, Iowa State University, Ames, IA 50011-2230, USA*
[b] *Laboratoire EM2C, CNRS, CentraleSupélec, Université Paris-Saclay, Grande Voie des Vignes, 92295 Châtenay Malabry, France*
[c] *Fédération de Mathématiques de l'Ecole Centrale Paris, Grande Voie des Vignes, 92295 Châtenay Malabry, France*

Abstract

The conditional quadrature method of moments (CQMOM) was introduced by Yuan and Fox [J. Comput. Phys. 230 (22), 8216–8246 (2011)] to reconstruct a velocity distribution function (VDF) from a finite set of its integer moments. The reconstructed VDF takes the form of a sum of weighted Dirac delta functions in velocity phase space, and provides a closure for the spatial flux term in the corresponding kinetic equation. The CQMOM closure for the flux leads to a weakly hyperbolic system of moment equations. In subsequent work [Chalons et al., Proceed. CTR Sum. Prog. 2010, 347–358 (2010)], the Dirac delta functions were replaced by Gaussian distributions, which make the moment system hyperbolic but at the added cost of dealing with continuous distributions. Here, a hyperbolic version of CQMOM is proposed that uses weighted Dirac delta functions. While the moment set employed for multi-Gaussian and conditional HyQMOM (CHyQMOM) are equivalent, the latter is able to access all of moment space whereas the former cannot (e.g. arbitrary values of the fourth-order velocity moment in 1-D phase space with two nodes). By making use of the properties of CHyQMOM in 2-D phase space, it is possible to control a symmetrical subset of the optimal moments [Fox, Indust. & Engng. Chem. Res. 48 (21), 9686–9696 (2009)]. Furthermore, the moment sets for 2-D problems are smaller for CHyQMOM than in the original CQMOM thanks to a judicious choice of the velocity abscissas in phase space.

Keywords: kinetic equation, quadrature-based moment methods, conditional quadrature method of moments, hyperbolic moment closures

1. Introduction

The physics of inertial particles can be described by a velocity density function (VDF) satisfying a kinetic equation. Solving such a kinetic equation relies on either a sample of discrete numerical parcels through a Lagrangian Monte-Carlo approach or on a moment approach resulting in a Eulerian system of conservation laws on velocity moments. For the latter, the main difficulty for particles with high Knudsen numbers where the VDF can be very far from equilibrium, is the closure of the free-transport term in the kinetic equation. One way to proceed is to use quadrature-based moment methods (QBMM) where the higher-order moments required for closure are evaluated from the lower-order transported moments using multi-dimensional quadratures [1, 2, 3]. In our previous work, we have developed the conditional quadrature method of moments (CQMOM) [4], leading to a well-behaved kinetic numerical scheme [5]. CQMOM has been shown to capture particle trajectory crossing (PTC) where the distribution in the exact kinetic equation remains at all times in the form of a sum of Dirac delta functions [4, 6, 7]. The moment system found with the CQMOM flux closure is weakly hyperbolic, leading to delta shocks when multiple PTC occur at the same

Email addresses: rodney.fox@iastate.edu (Rodney O. Fox), frederique.laurent@centralesupelec.fr (Frédérique Laurent), aymeric.vie@centralesupelec.fr (Aymeric Vié)

location. To achieve hyperbolicity, a multi-Gaussian QBMM closure was proposed [8]. However, this closure cannot access all of moment space [9, 10, 11] due to the form of Gaussian distribution (e.g. the two-node closure cannot represent fourth-order velocity moments larger than a Gaussian distribution). Moreover, working with a continuous representation of the VDF loses the discrete velocity representation of CQMOM [12].

The purpose of this work is to introduce a hyperbolic QMOM reconstruction of the VDF (HyQMOM in 1-D and CHyQMOM is 2 phase space) that circumvents the known shortcomings of the multi-Gaussian closure while retaining a hyperbolic moment system. In one-dimensional (1-D) phase space, the moment set controlled by HyQMOM is exactly the same as with the multi-Gaussian closure, namely integer moments up to order $2N$ where N is the number of nodes. Here we analyze the HyQMOM for $N = 2$ and 3, extend it to 2-D phase space using CQMOM, and apply it to the solution of a kinetic equation. The remainder of the work is organized as follows. In §2 the HyQMOM is described. In §3, we provide an in-depth description of the application to 1-D kinetic equations and the mathematical properties of two- and three-node HyQMOM. In §4, we extend HyQMOM to a 2-D phase space using a modified version of CQMOM. In §5 we describe the application of CHyQMOM to 2-D kinetic equations. Example applications are provided in §6. Finally, conclusions are drawn in §7. Mathematical details on moment methods and extension of CHyQMOM to higher-order moments are provided in the appendices.

2. HyQMOM

Consider a VDF $f(u)$ defined for $u \in \mathbb{R}$. Let us assume that the moments of f defined by

$$M_k := \int_{\mathbb{R}} f(u) u^k \, \mathrm{d}u \quad \text{for } k \in \{0, 1, \ldots, \max(1, 2N-2)\} \tag{1}$$

are finite and known. Let us define the central moments by

$$C_k := \frac{1}{M_0} \int_{\mathbb{R}} f(u)(u-\bar{u})^k \, \mathrm{d}v \quad \text{for } k \in \{0, 1, \ldots, \max(1, 2N-2)\} \tag{2}$$

where $\bar{u} = M_1/M_0$. By definition, $C_0 = 1$ and $C_1 = 0$. The next central moment $C_2 \geq 0$ is the velocity variance. For any $k \geq 0$, the central moment C_k depends uniquely on the moments $\{M_0, M_1, \ldots, M_k\}$. For nonnegative $f(u)$, the moments are said to be realizable. The realizability of a finite set of moments can be checked using Hankel matrix determinants as described in Appendix A. In particular, up to fourth order the central moments reside in the interior of moment space if $C_2 > 0$ and $C_4 > C_2^2 + C_3^2/C_2$. Hereinafter we will assume that the moment set under consideration is realizable.

2.1. Definition of HyQMOM

HyQMOM provides a discrete approximation f^a defined such that

$$C_k = C_k^a := \frac{1}{M_0} \int_{\mathbb{R}} f^a(u)(u-\bar{u})^k \, \mathrm{d}u \quad \text{for } k \in \{0, 1, \ldots, \max(1, 2N-2)\}, \tag{3}$$

and the central moment C_{2N-1} is a function of $(C_2, C_3, \ldots, C_{2N-2})$. More precisely, f^a has the form:

$$f^a(u) = M_0 \sum_{\alpha=1}^{N} \rho_\alpha \delta_{u_\alpha + \bar{u}}(u) \tag{4}$$

where $\delta_{u_\alpha+\bar{u}}(u)$ is the Dirac delta function centered at $u_\alpha + \bar{u}$, and the N weights ρ_α and the N velocity abscissas u_α are determined from the first $2N-1$ integer moments of f^a by (3), which is equivalent to

$$C_k = \sum_{\alpha=1}^{N} \rho_\alpha u_\alpha^k \quad \text{for } k \in \{0, 1, \ldots, 2N-1\}. \tag{5}$$

In comparison to QMOM, HyQMOM fixes the central moment C_{2N-1}, instead of computing it from moments up to M_{2N-1}, such that the 1-D moment system in §3.1 is hyperbolic. The algorithm for computing f^a from the moment set $\{C_0, \ldots, C_{2N-1}\}$ using (5) is exactly the same as with QMOM [4, 13]. The solution to (5) with $N = 1$ is trivial. As shown below, for $N = 2$ and 3 the weights ρ_α and velocity abscissas u_α can be found analytically. Note that due to the form of (4), the Hankel matrix $\mathbf{H}_N = 0$, which effectively constraints the even-order moment C_{2N}. The odd-order central moments have no such constraints.

2.2. Two-node HyQMOM

The function f^a has exact moments M_i^a of orders $i = 0, 1, 2$ given by (5) with $N = 2$. The four unknowns ρ_1, ρ_2, u_1, u_2 are found by solving the nonlinear system $C_i = C_i^a,\ i = 0, \ldots, 3$:

$$\begin{aligned} 1 &= \rho_1 + \rho_2, \\ 0 &= \rho_1 u_1 + \rho_2 u_2, \\ C_2 &= \rho_1 u_1^2 + \rho_2 u_2^2, \\ C_3 &= \rho_1 u_1^3 + \rho_2 u_2^3, \end{aligned} \tag{6}$$

where $C_3 = 0$. Note that the abscissas can be rescaled by $\sqrt{C_2}$ and thus (6) has no independent parameters. It remains to prove that this system is well posed in the following proposition.

Proposition 1 (Two-node HyQMOM)**.** *For moment set* $\mathbf{M} = (M_0, M_1, M_2)^t$ *such that* $M_0 > 0$*, define the central moment*

$$C_2 = \frac{M_0 M_2 - M_1^2}{M_0^2}$$

and set $C_3 = 0$*. System (6) is well defined on the phase space* Ω *given by*

$$\Omega = \{\mathbf{M},\ M_0 > 0 \text{ and } C_2 > 0\}.$$

Setting $\mathbf{U} = (\rho_1, \rho_2, u_1, u_2)^t$*, the function* $\mathbf{U} = \mathbf{U}(\mathbf{M})$ *is one-to-one and onto.*

Proof. In the case $C_2 > 0$, using the second equation, the last two equations in (6) yield

$$\begin{aligned} \rho_1 u_1 (u_1 - u_2) &= C_2, \\ u_1 + u_2 &= 0. \end{aligned} \tag{7}$$

Using the first equation in (6), these equations then yield

$$\begin{aligned} \rho_1 = \rho_2 &= \frac{1}{2}, \\ u_1 = -u_2 &= \sqrt{C_2}. \end{aligned} \tag{8}$$

The weights are non-negative and the abscissas are always real-valued. This concludes the proof.

If $M_0 = 0$, then $\mathbf{M}$ is realizable only if $M_1 = M_2 = 0$. When $C_2 = 0$, two-node HyQMOM reduces to one-node QMOM.

2.3. Three-node HyQMOM

The function f^a has exact central moments C_i^a of orders $i = 0, ..., 4$ given by (5) with $N = 3$. The six unknowns ρ_1, ρ_2, ρ_3, u_1, u_2, u_3 are found by solving the nonlinear system

$$\begin{aligned} 1 &= \rho_1 + \rho_2 + \rho_3, \\ 0 &= \rho_1 u_1 + \rho_2 u_2 + \rho_3 u_3, \\ C_2 &= \rho_1 u_1^2 + \rho_2 u_2^2 + \rho_3 u_3^2, \\ C_3 &= \rho_1 u_1^3 + \rho_2 u_2^3 + \rho_3 u_3^3, \\ C_4 &= \rho_1 u_1^4 + \rho_2 u_2^4 + \rho_3 u_3^4, \\ C_5 &= \rho_1 u_1^5 + \rho_2 u_2^5 + \rho_3 u_3^5, \end{aligned} \tag{9}$$

where $C_5 = \frac{C_3}{C_2^2}\left(2C_2C_4 - C_3^2\right)$ so that $u_2 = 0$. Note again that the abscissas can be rescaled by $\sqrt{C_2}$ and thus (9) depends only on the two dimensionless moments $q = C_3/C_2^{3/2}$ and $\eta = C_4/C_2^2$. It remains to prove that this system is well posed in the following proposition.

Proposition 2 (Three-node HyQMOM)**.** *For moment set* $\mathbf{M} = (M_0, M_1, M_2, M_3, M_4)^t$ *such that* $M_0 > 0$*, define the central moments*

$$C_2 = \frac{M_0M_2 - M_1^2}{M_0^2}, \quad C_3 = \frac{M_0^2M_3 - 3M_0M_1M_2 + 2M_1^3}{M_0^3},$$
$$C_4 = \frac{M_0^3M_4 - 4M_0^2M_1M_3 + 6M_0M_1^2M_2 - 3M_1^4}{M_0^4}$$

and set $C_5 = \frac{C_3}{C_2^2}\left(2C_2C_4 - C_3^2\right)$*. System (9) is well defined on the phase space* Ω *given by*

$$\Omega = \left\{\mathbf{M},\ M_0 > 0,\ C_2 > 0 \text{ and } C_4 \geq C_2^2 + \frac{C_3^2}{C_2}\right\}.$$

Setting $\mathbf{U} = (\rho_1, \rho_2, \rho_3, \rho_1u_1, \rho_3u_3)^t$*, the function* $\mathbf{U} = \mathbf{U}(\mathbf{M})$ *is one-to-one and onto.*

Proof. Solving (9) with $u_2 = 0$ is equivalent to solving the following nonlinear system in $(\rho_1^*, \rho_2, \rho_3^*, u_1, u_3)$:

$$\begin{aligned}
\rho_2 &= 1 - \rho_1^*/u_1 - \rho_3^*/u_3,\\
\rho_1^* + \rho_3^* &= 0,\\
\rho_1^*u_1 + \rho_3^*u_3 &= C_2,\\
\rho_1^*u_1^2 + \rho_3^*u_3^2 &= C_3,\\
\rho_1^*u_1^3 + \rho_3^*u_3^3 &= C_4,\\
C_5 &= \rho_1^*u_1^4 + \rho_3^*u_3^4.
\end{aligned} \tag{10}$$

In the case $C_2 > 0$, the last five equations yield

$$\begin{aligned}
\rho_3^* &= -\rho_1^*,\\
\rho_1^*(u_1 - u_3) &= C_2,\\
u_1 + u_3 &= C_3/C_2 = C_2^{1/2}q,\\
u_1^2 + u_1u_3 + u_3^2 &= C_4/C_2 = C_2\eta,\\
C_5 &= C_3\left(u_1^2 + u_3^2\right).
\end{aligned} \tag{11}$$

The last three equations then yield

$$\begin{aligned}
u_1 &= C_2^{1/2}\frac{1}{2}\left(q - \sqrt{4\eta - 3q^2}\right),\\
u_3 &= C_2^{1/2}\frac{1}{2}\left(q + \sqrt{4\eta - 3q^2}\right),
\end{aligned} \tag{12}$$

and

$$C_5 = C_2^{5/2}q\left(2\eta - q^2\right), \tag{13}$$

which give real-valued abscissas with $u_1 < 0$ and $u_3 > 0$ when $4\eta \geq 3q^2$. The corresponding weights are

$$\rho_1 = \frac{-C_2^{1/2}}{u_1\sqrt{4\eta - 3q^2}}, \quad \rho_2 = 1 + \frac{C_2}{u_1u_3}, \quad \rho_3 = \frac{C_2^{1/2}}{u_3\sqrt{4\eta - 3q^2}}. \tag{14}$$

The weights are non-negative if $\eta \geq 1 + q^2$, which is the realizability condition for $\mathbf{M}$ and, hence, the abscissas found from (12) are always real-valued. This concludes the proof.

If $M_0 = 0$, then $\mathbf{M}$ is realizable only if $M_1 = M_2 = M_3 = M_4 = 0$. If $C_2 = 0$, then $\mathbf{M}$ is realizable only if $C_3 = C_4 = 0$, in which case $\rho_1 = \rho_3 = 0$. When $C_2C_4 = C_2^3 + C_3^2$, the weight $\rho_2 = 0$ and, hence, the three-node HyQMOM reduces to two-node QMOM at the boundary of moment space.

3. Application of HyQMOM to 1-D kinetic equations

We first introduce HyQMOM for the VDF $f(t,x,u)$ in 1-D phase/real space for the kinetic equation:

$$\partial_t f + u\partial_x f + \partial_u(\mathcal{A}f) = 0, \quad t > 0,\, x \in \mathbb{R},\, u \in \mathbb{R}, \tag{15}$$

with initial condition $f(0,x,u) = f_0(x,u)$. The acceleration $\mathcal{A}$ is a real-valued function of u. The exact solution for free transport (when $\mathcal{A} = 0$) is given by $f(t,x,u) = f(0,x-ut,u) = f_0(x-ut,u)$. In this work, we seek an approximation of $f(t,x,u)$ in the form of HyQMOM with weights $\rho_\alpha(t,x) > 0$, velocity abscissas $u_\alpha(t,x)$ for $\alpha \in (1,\ldots,N)$ and $N = 3$. These weights and abscissas are determined from the 1-D moment transport equations.

3.1. 1-D moment transport equations

Defining the i^{th}-order moment:

$$M_i(t,x) = \int_{\mathbb{R}} f(t,x,u)u^i \,\mathrm{d}u, \quad i = 0,\ldots,K; \quad K \in \mathbb{N};$$

the associated governing equations are easily obtained from (15) after multiplication by u^i and integration over u:

$$\partial_t M_i + \partial_x M_{i+1} = \overline{\mathcal{A}}_i,\ i \geq 0,$$

where the (unclosed)[1] moment acceleration term is

$$\overline{\mathcal{A}}_i = -\int_{\mathbb{R}} i\mathcal{A}(u)f(t,x,u)u^{i-1} \,\mathrm{d}u. \tag{16}$$

For simplicity, we will focus our attention on the five-moment model and its abstract form:

$$\begin{aligned}
&\partial_t M_0 + \partial_x M_1 = 0,\\
&\partial_t M_1 + \partial_x M_2 = \overline{\mathcal{A}}_1,\\
&\partial_t M_2 + \partial_x M_3 = \overline{\mathcal{A}}_2, \quad \Longrightarrow \quad \partial_t \mathbf{M} + \partial_x \mathbf{F}(\mathbf{M}) = \overline{\mathbf{A}},\\
&\partial_t M_3 + \partial_x M_4 = \overline{\mathcal{A}}_3,\\
&\partial_t M_4 + \partial_x \overline{M}_5 = \overline{\mathcal{A}}_4.
\end{aligned} \tag{17}$$

with $\mathbf{M} = (M_0,\ldots,M_4)^t$, $\mathbf{F}(\mathbf{M}) = (M_1,\ldots,M_4,\overline{M}_5)^t$ and $\overline{\mathbf{A}} = (0,\overline{\mathcal{A}}_1,\ldots,\overline{\mathcal{A}}_4)^t$. This model is closed provided that $\overline{M}_5$ and $\overline{\mathbf{A}}$ are defined as functions of $\mathbf{M}$. Here we propose to define these functions using three-node HyQMOM. Note that unlike previous five-moment closures [9, 11], three-node HyQMOM in (17) is well defined over the entire (realizable) moment space $\mathbf{M}$.

3.2. Mathematical properties of moment system with HyQMOM

The following theorem addresses an important mathematical property of system (17).

Theorem 1 (Hyperbolicity)**.** *Assuming that the vector* $\mathbf{M} = (M_0,M_1,M_2,M_3,M_4)^t$ *lives in the space* Ω *defined in Proposition 2, system* (17) *with the three-node HyQMOM closure is hyperbolic.*

[1]The acceleration terms will be closed if $\mathcal{A}$ is affine: $\mathcal{A}(t,x,u) = -a(t,x)u + b(t,x)$, in which case the moment acceleration term can be written as $\overline{\mathcal{A}}_k = k(aM_k - bM_{k-1})$. In gas–particle flows, this limit corresponds to Stokes drag in a stationary fluid.

Proof. It is shown in Proposition 2 that one can define $U = (\rho_1, \rho_2, \rho_3, \rho_1 u_1, \rho_3 u_3)^t$, the vector of the reconstruction variables, using the three-node HyQMOM closure.

The Jacobian matrix of system (17) is

$$J = \begin{bmatrix} 0 & 1 & 0 & 0 & 0 \\ 0 & 0 & 1 & 0 & 0 \\ 0 & 0 & 0 & 1 & 0 \\ 0 & 0 & 0 & 0 & 1 \\ \alpha & \beta & \gamma & \delta & \epsilon \end{bmatrix}$$

where $(\alpha, \beta, \gamma, \delta, \epsilon) = \dfrac{D\overline{M}_5}{D\mathbf{M}}$ and $\overline{M}_5 = M_0 \left[\rho_1(\bar{u} + u_1)^5 + \rho_2 \bar{u}^5 + \rho_3(\bar{u} + u_3)^5\right]$. The corresponding characteristic polynomial is

$$P(X) = -X^5 + \epsilon\, X^4 + \delta\, X^3 + \gamma\, X^2 + \beta\, X + \alpha.$$

After some tedious algebra, one obtains

$$C_2^{-5/2} P\left(\bar{u} + \sqrt{C_2} Y\right) = -Y^5 + 2qY^4 + \left(2\eta - 3q^2\right) Y^3 - 2q\left(\eta - q^2\right) Y^2 - \left(\eta - q^2\right) Y$$

with $q = C_3/C_2^{3/2}$ and $\eta = C_4/C_2^2$. This polynomial function P then admits five roots:

$$\bar{u}, \quad \bar{u} + \sqrt{C_2}\frac{1}{2}\left(q \pm \sqrt{4\eta - 3q^2 \pm 4\sqrt{\left(\eta - q^2\right)\left(\eta - q^2 - 1\right)}}\right). \tag{18}$$

Thanks to the realizability constraint $\eta > 1 + q^2$, it is easy to show that all roots are distinct and real-valued. This concludes the proof.

If $\eta = 1 + q^2$, the moments are on the boundary of moment space and system (17) is weakly hyperbolic. Using the same procedure as in Theorem 1, it can be shown that the moment system resulting from two-node HyQMOM is hyperbolic when $C_2 > 0$.

3.3. Kinetic-based flux

In our numerical implementation to solve (17), the spatial fluxes $\mathbf{F}(\mathbf{M})$ are computed using a kinetic-based definition:

$$F_i(t,x) = \int_0^\infty f(t,x,u) u^{i+1}\, \mathrm{d}u + \int_{-\infty}^0 f(t,x,u) u^{i+1}\, \mathrm{d}u, \quad i = 0, \ldots, 4; \tag{19}$$

where the decomposition into positive and negative directions is used to define the flux function as proposed in [5, 14]. The numerical representation of the flux function is a critical point in moment transport methods [1, 2, 3, 7, 15] because only *realizable* moment sets can be successfully inverted.

Formally, for non-degenerate cases we close (19) using

$$F_i(t,x) = M_0 \sum_{\alpha=0}^{4} w_\alpha \left[\max\left(0, \lambda_\alpha\right)^{i+1} + \min\left(0, \lambda_\alpha\right)^{i+1}\right], \quad i = 0, \ldots, 4, \tag{20}$$

where λ_α are the eigenvalues in (18) with $\lambda_0 = \bar{u}$. The weights w_α are found by solving the moment problem:

$$M_0 \begin{bmatrix} 1 & 1 & 1 & 1 & 1 \\ \lambda_0 & \lambda_1 & \lambda_2 & \lambda_3 & \lambda_4 \\ \lambda_0^2 & \lambda_1^2 & \lambda_2^2 & \lambda_3^2 & \lambda_4^2 \\ \lambda_0^3 & \lambda_1^3 & \lambda_2^3 & \lambda_3^3 & \lambda_4^3 \\ \lambda_0^4 & \lambda_1^4 & \lambda_2^4 & \lambda_3^4 & \lambda_4^4 \end{bmatrix} \begin{bmatrix} w_0 \\ w_1 \\ w_2 \\ w_3 \\ w_4 \end{bmatrix} = \begin{bmatrix} M_0 \\ M_1 \\ M_2 \\ M_3 \\ M_4 \end{bmatrix},$$

which is equivalent to $w_0 = 0$ and

$$\begin{bmatrix} \varphi_1 & \varphi_2 & \varphi_3 & \varphi_4 \\ \varphi_1^2 & \varphi_2^2 & \varphi_3^2 & \varphi_4^2 \\ \varphi_1^3 & \varphi_2^3 & \varphi_3^3 & \varphi_4^3 \\ \varphi_1^4 & \varphi_2^4 & \varphi_3^4 & \varphi_4^4 \end{bmatrix} \begin{bmatrix} w_1 \\ w_2 \\ w_3 \\ w_4 \end{bmatrix} = \begin{bmatrix} 0 \\ 1 \\ q \\ \eta \end{bmatrix} \tag{21}$$

where $\varphi_\alpha = (\lambda_\alpha - \bar{u})/\sqrt{C_2}$. Using the characteristic polynomial from Theorem 1, it is straightforward to show that

$$C_5 = \sum_{\alpha=1}^{3} \rho_\alpha u_\alpha^5 = C_2^{5/2} \sum_{\alpha=1}^{4} w_\alpha \varphi_\alpha^5 = C_2^{5/2} q(2\eta - q^2),$$

and thus that both quadratures yield the same closure for M_5 (as well as for M_0 to M_4). For the degenerate case where $\eta = 1 + q^2$, the three distinct eigenvalues are used in (20). Finally, for the degenerate case where $C_2 = 0$, the single eigenvalue $\bar{u}$ is used.

To design a first-order scheme, this decomposition is sufficient as it corresponds to an upwind scheme at the kinetic level. For a high-order scheme [7], the spatial fluxes can be found from (20) by employing a high-order spatial reconstruction for $M_0 w_\alpha$ and a first-order reconstruction for the abscissas λ_α. In summary, the numerical fluxes are computed as follows:

1. Given moments $\mathbf{M}$, compute $\bar{u}$, C_2, q, η, λ_α, and w_α.
2. Compute kinetic-based fluxes from (20).
3. Compute finite-volume numerical moment fluxes as described in [7].

4. Extension of HyQMOM to 2-D phase space

Consider a 2-D phase space with VDF $f(\mathrm{v})$ for $\mathrm{v} = (u, v)^t$ and define the bivariate moments

$$M_{i,j} := \int_{\mathbb{R}^2} f(\mathrm{v}) u^i v^j \,\mathrm{dv},\ i, j = 0, \ldots, K;\ K \in \mathbb{N}. \tag{22}$$

If $M_{0,0} > 0$, the bivariate central moments are defined by

$$C_{i,j} := \frac{1}{M_{0,0}} \int_{\mathbb{R}^2} f(\mathrm{v})(u - \bar{u})^i (v - \bar{v})^j \,\mathrm{dv},\ i, j = 0, \ldots, K;\ K \in \mathbb{N}; \tag{23}$$

where $\bar{u} = M_{1,0}/M_{0,0}$ and $\bar{v} = M_{0,1}/M_{0,0}$. Assuming that these moments are realizable, which can be checked using moment matrices [16], in the following we propose a bivariate extension of HyQMOM using ideas from CQMOM [4].

4.1. Definition of 2-D CHyQMOM

For clarity, we limit our discussion here to nine-node quadrature in 2-D phase space. Nevertheless, the same methodology can be used to develop the formulas for more nodes. For the nine-node quadrature, we define an approximate bivariate VDF by

$$f^a(\mathrm{v}) := M_{0,0} \sum_{\alpha=1}^{N} \rho_\alpha \delta_{\bar{u}+u_\alpha}(u) \sum_{\beta=1}^{N} \rho_{\alpha\beta} \delta_{\bar{v}+\bar{v}_\alpha+v_{\alpha\beta}}(v) \tag{24}$$

where $N = 3$, and the parameters $\{\rho_1, \rho_2, \rho_3, u_1, u_3\}$ ($u_2 = 0$) are determined using the three-node HyQMOM algorithm in §2.3 from the moments $\{M_{0,0}, M_{1,0}, M_{2,0}, M_{3,0}, M_{4,0}\}$. In (24), $\bar{v}_\alpha$ and $v_{\alpha\beta}$ are found from the moments $\{M_{1,1}, M_{0,1}, M_{0,2}, M_{0,3}, M_{0,4}\}$ as described next. The total number of nodes in 2-D phase space is thus nine for nondegenerate cases.

As shown in §3.3, for the spatial fluxes a quadrature based on the eigenvalues is needed. Using the flux-based quadrature, the VDF reconstruction is

$$f^a(\mathrm{v}) := M_{0,0} \sum_{\alpha=0}^{N_\lambda-1} w_\alpha \delta_{\lambda_\alpha}(u) \sum_{\beta=1}^{N} \rho_{\alpha\beta} \delta_{\bar{v}+\bar{v}_\alpha+v_{\alpha\beta}}(v) \tag{25}$$

where $N_\lambda = 2N-1$ is the number of eigenvalues $\lambda_\alpha = \bar{u} + \sqrt{C_{2,0}}\varphi_\alpha$. The formulas in this section and in §4.2 are derived using the notation in (24), but equivalent formulas can be found for (25) by substituting w_α for ρ_α and φ_α for $u_\alpha/C_{2,0}^{1/2}$. The latter are needed for computing the kinetic-based fluxes in §5.3.

The correlation parameters $\bar{v}_\alpha = a_0 + a_1 u_\alpha$ in (24) are defined to have the following properties:

$$\sum_{\alpha=1}^{N} \rho_\alpha \bar{v}_\alpha = C_{0,1} = 0, \quad \sum_{\alpha=1}^{N} \rho_\alpha u_\alpha \bar{v}_\alpha = C_{1,1}. \tag{26}$$

This yields $a_0 = 0$ and $a_1 = C_{1,1}/C_{2,0}$, and thus

$$\bar{v}_\alpha = \frac{C_{1,1}}{C_{2,0}} u_\alpha. \tag{27}$$

Note that $\bar{v}_2 = 0$ because $u_2 = 0$.

The central moments found from (24) are

$$C_{i,j} = \sum_{\alpha=1}^{N} \rho_\alpha u_\alpha^i \sum_{\beta=1}^{N} \rho_{\alpha\beta} \left(\bar{v}_\alpha + v_{\alpha\beta}\right)^j. \tag{28}$$

A binomial expansion then leads to

$$C_{i,j} = \sum_{j_1=0}^{j} \binom{j}{j_1} \sum_{\alpha=1}^{N} \rho_\alpha u_\alpha^i \bar{v}_\alpha^{j-j_1} C_{j_1|\alpha} \tag{29}$$

where the conditional central moments are

$$C_{j|\alpha} := \sum_{\beta=1}^{N} \rho_{\alpha\beta} v_{\alpha\beta}^j. \tag{30}$$

It follows immediately from (29) that $C_{0|\alpha} = 1$. By choosing $C_{2,1} = C_{1,1}C_{3,0}/C_{2,0}$, we find $C_{1|\alpha} = 0$. The form of (29) leads to the following moment-inversion algorithm based on CQMOM.

4.2. Moment-inversion algorithm for 2-D, nine-node CHyQMOM

The first step uses the univariate moments $M_{i,0}$ with the algorithm in §2.3 for 1-D, three-node HyQMOM to find $\{\rho_1, \rho_2, \rho_3, u_1, u_3\}$. There are three possible cases: (1) a nondegenerate case with $u_1 \neq u_3$ and $\rho_2 > 0$, (2) a degenerate case with $\rho_2 = 1$, (3) a degenerate case with $\rho_2 = 0$. Case (2) occurs when the univariate moments $M_{i,0}$ have zero variance ($C_{2,0} = 0$). Case (3) occurs when the univariate moments $M_{i,0}$ are on the boundary of moment space ($C_{2,0} > 0$ and $C_{2,0}C_{4,0} = C_{2,0}^3 + C_{3,0}^2$).

4.2.1. Case (2)

For this case, we define a 2-D, three-node CHyQMOM by

$$f^a(\mathrm{v}) := M_{0,0} \delta_{\bar{u}}(u) \sum_{\beta=1}^{3} \rho_\beta \delta_{\bar{v}+v_\beta}(v). \tag{31}$$

The algorithm in §2.3 for three-node HyQMOM is employed with the moment set $\{1, 0, C_{0,2}, C_{0,3}, C_{0,4}\}$ to find the parameters $\{\rho_1, \rho_2, \rho_3, v_1, v_3\}$ ($v_2 = 0$).

4.2.2. Cases (1) and (3)

The parameters $\{\rho_{\alpha\,1}, \rho_{\alpha\,2}, \rho_{\alpha\,3}, v_{\alpha\,1}, v_{\alpha\,2},\}$ are determined from the conditional moments $\{C_{0|\alpha}, C_{1|\alpha}, C_{2|\alpha}, C_{3|\alpha}, C_{4|\alpha}\}$ using the three-node HyQMOM in §2.3. As shown above, $C_{0|\alpha} = 1$, and $C_{1|\alpha} = 0$ when $C_{2,1} = C_{1,1}C_{3,0}/C_{2,0}$. Thus we compute

$$C_{2|\alpha} = C_{0,2}\left(b_0 + b_1 \frac{u_\alpha}{C_{2,0}^{1/2}}\right) \tag{32}$$

from (29) using $\{C_{0,2}, C_{1,2}\}$ by choosing $C_{1,2} = C_{1,1}C_{0,3}/C_{0,2}$. This yields

$$\begin{aligned} \sum_{\alpha=1}^{3} \rho_\alpha C_{2|\alpha} &= C_{0,2}b_0 = C_{0,2} - \frac{C_{1,1}^2}{C_{2,0}} \quad \text{or} \quad b_0 = 1 - \varrho^2, \\ \sum_{\alpha=1}^{3} \rho_\alpha u_\alpha C_{2|\alpha} &= b_1 C_{2,0}^{1/2} C_{0,2} = C_{1,1}\frac{C_{0,3}}{C_{0,2}} - \frac{C_{1,1}^2}{C_{2,0}^2}C_{3,0} \quad \text{or} \quad b_1 = \varrho(q_2 - \varrho q_1) \end{aligned} \tag{33}$$

where $\varrho = C_{1,1}/\sqrt{C_{2,0}C_{0,2}}$, $q_1 = C_{3,0}/C_{2,0}^{3/2}$, and $q_2 = C_{0,3}/C_{0,2}^{3/2}$. If one of the conditional variances is null, then b_1 is limited such that all conditional variances are non-negative.

The conditional moments $C_{3|\alpha}$ and $C_{4|\alpha}$ are found from $\{C_{0,3}, C_{0,4}\}$ by assuming that they depend on α through $C_{2|\alpha}$: $C_{3|\alpha} = q^\star C_{2|\alpha}^{3/2}$ and $C_{4|\alpha} = \eta^\star C_{2|\alpha}^2$. This yields the following relations for $q^\star$ and $\eta^\star$:

$$q^\star = \left[\sum_{\alpha=1}^{3} \rho_\alpha \left(C_{2|\alpha}^\dagger\right)^{3/2}\right]^{-1} \left[2\varrho^3 q_1 + (1 - 3\varrho^2)q_2\right], \tag{34}$$

where $C_{2|\alpha}^\dagger = C_{2|\alpha}/C_{0,2}$, and

$$\eta^\star = \left[\sum_{\alpha=1}^{3} \rho_\alpha \left(C_{2|\alpha}^\dagger\right)^{2}\right]^{-1} \left[\eta_2 - \varrho^4\eta_1 - 6\varrho[\varrho(1-\varrho^2) + (q_2 - \varrho q_1)q_1] - 4\varrho q^\star \sum_{\alpha=1}^{3} \rho_\alpha u_\alpha^\dagger \left(C_{2|\alpha}^\dagger\right)^{3/2}\right] \tag{35}$$

where $u_\alpha^\dagger = u_\alpha/C_{2,0}^{1/2}$, $\eta_1 = C_{4,0}/C_{2,0}^2$ and $\eta_2 = C_{0,4}/C_{0,2}^2$.

In the limit of perfect correlation, $|\varrho| = 1$, $q_2 = \varrho q_1$ and $\eta_2 = \varrho^2\eta_1$, and thus $q^\star = 0$ and $\eta^\star = 0$. For uncorrelated variables, $\varrho = 0$, $q^\star = q_2$ and $\eta^\star = \eta_2$. Otherwise, the realizability of $C_{4|\alpha}$ requires that $\eta^\star \geq 1 + (q^\star)^2$. If this condition is not met, then $q^\star$ and $\eta^\star$ are projected to the realizability curve $\eta^\star = 1 + (q^\star)^2$ along the direction of the Gaussian moments (i.e., $q^\star = 0$ and $\eta^\star = 3$). Three-node HyQMOM can then be applied for each α to find the remaining parameters.

4.3. Other remarks

The moment-inversion algorithm described above is able to recover ten velocity moments:

$$\mathbf{M} = \begin{bmatrix} M_{0,0} & M_{0,1} & M_{0,2} & M_{0,3} & M_{0,4} \\ M_{1,0} & M_{1,1} & & & \\ M_{2,0} & & & & \\ M_{3,0} & & & & \\ M_{4,0} & & & & \end{bmatrix}, \tag{36}$$

which is a symmetrical subset of the optimal moments [17]. However, the reconstruction in (24) in not unique for this moment set, which is not surprising since a general 2-D, nine-node quadrature has 27 degrees of freedom [17]. For example, transposing the moments $M_{i,j} \Rightarrow M_{j,i}$ will generally lead to a different set of reconstruction parameters. The difference between the two reconstructions will lead to different closures for the moments not incluced in $\mathbf{M}$. The advantage of using CHyQMOM over CQMOM [4] and second-order

closures [8] for approximating solutions to kinetic equations is that the system will be hyperbolic, while at the same time allowing for particle-trajectory crossing [1, 2].

The reader can note that the formulas developed in this section for 2-D, nine-node CHyQMOM can be extended to third-order moments by including $M_{1,2}$ and $M_{2,1}$ in $\mathbf{M}$ in a relatively straightforward manner (see Appendix B).

5. Application of nine-node CHyQMOM to kinetic equations

Consider a 2-D velocity phase space with VDF $f(t, \mathrm{x}, \mathrm{v})$ for $\mathrm{x} = (x, y)^t$ and $\mathrm{v} = (u, v)^t$ that satisfies the kinetic equation

$$\partial_t f + \mathrm{v} \cdot \partial_{\mathrm{x}} f + \partial_{\mathrm{v}} \cdot (\mathbf{A} f) = 0, \quad t > 0,\, \mathrm{x} \in \mathbb{R}^2,\, \mathrm{v} \in \mathbb{R}^2, \tag{37}$$

with initial condition $f(0, \mathrm{x}, \mathrm{v}) = f_0(\mathrm{x}, \mathrm{v})$. The acceleration $\mathbf{A} = (\mathcal{A}_x, \mathcal{A}_y)^t$ is a real-valued function of v. With a 2-D velocity phase space, we approximate the solution to f using CHyQMOM for the bivariate moments. In this work, we will consider only the *minimal* CHyQMOM in §4 that uses nine nodes in the 2-D velocity phase space. Nonetheless, the extension to more than nine nodes would be analogous to the algorithm presented here.

5.1. 2-D moment transport equations

Defining the bivariate moments

$$M_{i,j}(t, \mathrm{x}) = \int_{\mathbb{R}^2} f(t, \mathrm{x}, \mathrm{v}) u^i v^j \,\mathrm{dv}, \;\; i, j = 0, \ldots, K; \;\; K \in \mathbb{N};$$

the associated governing equations are easily obtained from (37):

$$\partial_t M_{i,j} + \partial_x M_{i+1,j} + \partial_y M_{i,j+1} = \overline{\mathcal{A}}_{i,j}, \quad i, j \geq 0;$$

where the (unclosed)[2] moment acceleration term is defined by

$$\overline{\mathcal{A}}_{i,j} = -\int_{\mathbb{R}^2} i \mathcal{A}_x(\mathrm{v}) f(t, \mathrm{x}, \mathrm{v}) u^{i-1} v^j \,\mathrm{dv} - \int_{\mathbb{R}^2} j \mathcal{A}_y(\mathrm{v}) f(t, \mathrm{x}, \mathrm{v}) u^i v^{j-1} \,\mathrm{dv}. \tag{38}$$

We will consider in this work the ten moments in (36):

$$\begin{aligned}
&\partial_t M_{0,0} + \partial_x M_{1,0} + \partial_y M_{0,1} = 0,\\
&\partial_t M_{1,0} + \partial_x M_{2,0} + \partial_y M_{1,1} = \overline{\mathcal{A}}_{1,0},\\
&\partial_t M_{0,1} + \partial_x M_{1,1} + \partial_y M_{0,2} = \overline{\mathcal{A}}_{0,1},\\
&\partial_t M_{2,0} + \partial_x M_{3,0} + \partial_y \overline{M}_{2,1} = \overline{\mathcal{A}}_{2,0},\\
&\partial_t M_{1,1} + \partial_x \overline{M}_{2,1} + \partial_y \overline{M}_{1,2} = \overline{\mathcal{A}}_{1,1},\\
&\partial_t M_{0,2} + \partial_x \overline{M}_{1,2} + \partial_y M_{0,3} = \overline{\mathcal{A}}_{0,2},\\
&\partial_t M_{3,0} + \partial_x M_{4,0} + \partial_y \overline{M}_{3,1} = \overline{\mathcal{A}}_{3,0},\\
&\partial_t M_{0,3} + \partial_x \overline{M}_{1,3} + \partial_y M_{0,4} = \overline{\mathcal{A}}_{0,3},\\
&\partial_t M_{4,0} + \partial_x \overline{M}_{5,0} + \partial_y \overline{M}_{4,1} = \overline{\mathcal{A}}_{4,0},\\
&\partial_t M_{0,4} + \partial_x \overline{M}_{1,4} + \partial_y \overline{M}_{0,5} = \overline{\mathcal{A}}_{0,4},
\end{aligned} \tag{39}$$

which requires a closure for the two third-order moments $\overline{M}_{2,1}$, $\overline{M}_{1,2}$, the two fourth-order moments $\overline{M}_{3,1}$, $\overline{M}_{1,3}$, the four fifth-order moments $\overline{M}_{5,0}, \overline{M}_{4,1}, \overline{M}_{1,4}, \overline{M}_{0,5}$, and the acceleration terms. We propose to define these closures by reconstructing f with nine-node CHyQMOM in (24) and (25). If unclosed, the acceleration term $\overline{\mathbf{A}}$ can be evaluated using f^a. In our numerical examples, Stokes drag is used so that $\overline{\mathbf{A}}$ is closed in terms of the transported moments, and operator splitting is used for the fluxes and the acceleration.

[2]The acceleration terms will be closed if $\mathbf{A}$ is a linear function of the form $(au, av)^t$, in which case the moment acceleration term can be written as $\overline{\mathcal{A}}_{i,j} = -a(i+j)M_{i,j}$. In gas-particle flows, this limit corresponds to Stokes drag in a stationary fluid.

5.2. Mathematical properties of 2-D moment system with nine-node CHyQMOM

Because we employ a dimensional splitting to solve (39), let us consider the transport part of the system in the x-direction for the moments used in the CHyQMOM reconstruction in (24):

$$\partial_t \mathbf{M} + \partial_x \mathbf{F}_x(\mathbf{M}) = 0 \tag{40}$$

with $\mathbf{M} = (M_{0,0}, M_{1,0}, M_{2,0}, M_{3,0}, M_{4,0}, M_{0,1}, M_{1,1}, M_{0,2}, M_{0,3}, M_{0,4})^t$ and

$$\mathbf{F}_x(\mathbf{M}) = (M_{1,0}, M_{2,0}, M_{3,0}, M_{4,0}, \overline{M}_{5,0}, M_{1,1}, \overline{M}_{2,1}, \overline{M}_{1,2}, \overline{M}_{1,3}, \overline{M}_{1,4})^t$$

where, using the flux-based quadrature in (25),

$$\begin{aligned}
\overline{M}_{5,0} &= M_{0,0} \sum_{\alpha=1}^{4} w_\alpha \lambda_\alpha^5, \\
\overline{M}_{2,1} &= M_{0,0} \sum_{\alpha=1}^{4} w_\alpha \lambda_\alpha^2 (\bar{v} + \bar{v}_\alpha), \\
\overline{M}_{1,2} &= M_{0,0} \sum_{\alpha=1}^{4} w_\alpha \lambda_\alpha \left[(\bar{v} + \bar{v}_\alpha)^2 + C_{2|\alpha} \right], \\
\overline{M}_{1,3} &= M_{0,0} \sum_{\alpha=1}^{4} w_\alpha \lambda_\alpha \left[(\bar{v} + \bar{v}_\alpha)^3 + 3(\bar{v} + \bar{v}_\alpha) C_{2|\alpha} + C_{3|\alpha} \right], \\
\overline{M}_{1,4} &= M_{0,0} \sum_{\alpha=1}^{4} w_\alpha \lambda_\alpha \left[(\bar{v} + \bar{v}_\alpha)^4 + 6(\bar{v} + \bar{v}_\alpha)^2 C_{2|\alpha} + 4(\bar{v} + \bar{v}_\alpha) C_{3|\alpha} + C_{4|\alpha} \right].
\end{aligned} \tag{41}$$

Here $\bar{v}_\alpha = (C_{1,1}/C_{2,0}^{1/2})\varphi_\alpha$, and the conditional moments $C_{j|\alpha}$ are defined using φ_α. The right-hand side of (41) can therefore be expressed in terms of the known central moments, $\bar{u}$, $\bar{v}$ and $M_{0,0}$. This observation leads to the following theorem.

Theorem 2 (Hyperbolicity)**.** *Assuming that the moment-inversion algorithm for 2-D, nine-node CHyQMOM for the vector* $\mathbf{M}$ *is non-degenerate, system (40) with this closure is hyperbolic for small* $|\varrho|$*.*

Proof. The additional fluxes for the 2-D problem can be written as

$$\begin{aligned}
\overline{M}_{2,1} &= \bar{v} M_{2,0} + M_{0,0} C_{1,1} \left(2\bar{u} + \frac{C_{3,0}}{C_{2,0}} \right), \\
\overline{M}_{1,2} &= \bar{u} M_{0,2} + M_{0,0} C_{1,1} \left(2\bar{v} + \frac{C_{0,3}}{C_{0,2}} \right), \\
\overline{M}_{1,3} &= \bar{u} M_{0,3} + 3\bar{v} M_{0,0} C_{1,1} \left(\bar{v} + \frac{C_{0,3}}{C_{0,2}} \right) + M_{0,0} \overline{C}_{1,3}, \\
\overline{M}_{1,4} &= \bar{u} M_{0,4} + 2\bar{v}^2 M_{0,0} C_{1,1} \left(2\bar{v} + 3\frac{C_{0,3}}{C_{0,2}} \right) + M_{0,0} \left(4\bar{v} \overline{C}_{1,3} + \overline{C}_{1,4} \right)
\end{aligned}$$

where, using the flux-based quadrature in (25),

$$\begin{aligned}
\overline{C}_{1,3} &= \sqrt{C_{2,0}} \sum_{\alpha=1}^{4} w_\alpha \varphi_\alpha \left(\bar{v}_\alpha^3 + 3\bar{v}_\alpha C_{2|\alpha} + C_{3|\alpha} \right), \\
\overline{C}_{1,4} &= \sqrt{C_{2,0}} \sum_{\alpha=1}^{4} w_\alpha \varphi_\alpha \left(\bar{v}_\alpha^4 + 6\bar{v}_\alpha^2 C_{2|\alpha} + 4\bar{v}_\alpha C_{3|\alpha} + C_{4|\alpha} \right),
\end{aligned}$$

and the eigenvalues φ_α are found from the eigenvalues λ_α of the 1-D system as shown below. These eigenvalues have the property $\sum_{\alpha=1}^4 w_\alpha \varphi_\alpha^k = C_{k,0}/C_{2,0}^{k/2}$ for $k = 0, 1, \ldots, 5$ where $C_{0,0} := 1$.

The Jacobian matrix J_{2D} of the fluxes is block triangular:

$$J_{2D} = \begin{bmatrix} J & 0 & 0 & 0 \\ X_1 & A_1 & 0 & 0 \\ X_2 & B_1 & A_2 & 0 \\ X_3 & C & B_2 & \lambda_{10} \end{bmatrix}$$

where J is the 5×5 Jacobian matrix given in Theorem 1, corresponding to the 1-D system. X_1 and X_2 are 2×5 matrices and X_3 is a 1×5 matrix. B_1 is a 2×2 matrix. C and B_2 are 1×2 matrices. A_1 is a 2×2 matrix given by

$$A_1 = \begin{bmatrix} 0 & 1 \\ \nu & \xi \end{bmatrix}$$

with

$$(\nu, \xi) = \frac{D\overline{M}_{2,1}}{D(M_{0,1}, M_{1,1})} = \left(C_{2,0} - \bar{u}^2 - \bar{u}\frac{C_{3,0}}{C_{2,0}}, 2\bar{u} + \frac{C_{3,0}}{C_{2,0}} \right).$$

A_2 is a 2×2 matrix given by

$$A_2 = \begin{bmatrix} a_{11} & a_{12} \\ a_{21} & a_{22} \end{bmatrix}$$

with

$$\begin{aligned} (a_{11}, a_{12}) &= \frac{D\overline{M}_{1,2}}{D(M_{0,2}, M_{0,3})} = \left(\bar{u} - \frac{C_{1,2}}{C_{0,2}} - 3\bar{v}\frac{C_{1,1}}{C_{0,2}}, \frac{C_{1,1}}{C_{0,2}} \right), \\ a_{21} &= \frac{\partial \overline{M}_{1,3}}{\partial M_{0,2}} = -3\bar{v}\frac{C_{1,2}}{C_{0,2}} - 9\bar{v}^2\frac{C_{1,1}}{C_{0,2}} + M_{0,0}\frac{\partial \overline{C}_{1,3}}{\partial M_{0,2}}, \\ a_{22} &= \frac{\partial \overline{M}_{1,3}}{\partial M_{0,3}} = \bar{u} + 3\bar{v}\frac{C_{1,1}}{C_{0,2}} + M_{0,0}\frac{\partial \overline{C}_{1,3}}{\partial M_{0,3}} \end{aligned}$$

where $C_{1,2} = C_{1,1}C_{0,3}/C_{0,2}$.

Using the dimensionless variables $\bar{u}^\dagger = \bar{u}/C_{2,0}^{1/2}$, $\bar{v}^\dagger = \bar{v}/C_{0,2}^{1/2}$, $\varrho = C_{1,1}/(C_{2,0}C_{0,2})^{1/2}$, $q_1 = C_{3,0}/C_{2,0}^{3/2}$, $q_2 = C_{0,3}/C_{0,2}^{3/2}$, $\eta_1 = C_{4,0}/C_{2,0}^2$, and $\eta_2 = C_{0,4}/C_{0,2}^2$, the partial derivatives can be expressed in dimensionless form as

$$\left(\frac{\partial \overline{C}_{1,3}}{\partial M_{0,2}}\right)^\dagger = \sum_{\alpha=1}^4 w_\alpha \varphi_\alpha \left[3\left(\varrho\varphi_\alpha + \frac{1}{2}q^\star \left(C_{2|\alpha}^\dagger\right)^{1/2} \right) \left(\frac{\partial C_{2|\alpha}}{\partial M_{0,2}}\right)^\dagger + \left(C_{2|\alpha}^\dagger\right)^{3/2} \left(\frac{\partial q^\star}{\partial M_{0,2}}\right)^\dagger \right],$$

$$\left(\frac{\partial \overline{C}_{1,3}}{\partial M_{0,3}}\right)^\dagger = \sum_{\alpha=1}^4 w_\alpha \varphi_\alpha \left[3\left(\varrho\varphi_\alpha + \frac{1}{2}q^\star \left(C_{2|\alpha}^\dagger\right)^{1/2} \right) \left(\frac{\partial C_{2|\alpha}}{\partial M_{0,3}}\right)^\dagger + \left(C_{2|\alpha}^\dagger\right)^{3/2} \left(\frac{\partial q^\star}{\partial M_{0,3}}\right)^\dagger \right]$$

where $C_{2|\alpha}^\dagger = C_{2|\alpha}/C_{0,2} = b_0 + b_1\varphi_\alpha$,

$$\left(\frac{\partial C_{2|\alpha}}{\partial M_{0,2}}\right)^\dagger = 1 - \varrho\left(3\bar{v}^\dagger + q_2\right)\varphi_\alpha, \quad \left(\frac{\partial C_{2|\alpha}}{\partial M_{0,3}}\right)^\dagger = \varrho\varphi_\alpha,$$

$$\left(\frac{\partial q^\star}{\partial M_{0,2}}\right)^\dagger = -3\left[\sum_{\alpha=1}^4 w_\alpha \left(C_{2|\alpha}^\dagger\right)^{3/2}\right]^{-1} \left[\bar{v}^\dagger - \varrho^2\left(3\bar{v}^\dagger + q_2\right) + \frac{1}{2}q^\star \sum_{\alpha=1}^4 w_\alpha \left(C_{2|\alpha}^\dagger\right)^{1/2} \left(\frac{\partial C_{2|\alpha}}{\partial M_{0,2}}\right)^\dagger \right],$$

and

$$\left(\frac{\partial q^\star}{\partial M_{0,3}}\right)^\dagger = \left[\sum_{\alpha=1}^4 w_\alpha \left(C_{2|\alpha}^\dagger\right)^{3/2}\right]^{-1} \left[1 - 3\varrho^2 - \frac{3}{2}q^\star \sum_{\alpha=1}^4 w_\alpha \left(C_{2|\alpha}^\dagger\right)^{1/2} \left(\frac{\partial C_{2|\alpha}}{\partial M_{0,3}}\right)^\dagger \right].$$

From Theorem 1, the matrix J is diagonalizable with five distinct eigenvalues $\lambda_\alpha = \bar{u} + \sqrt{C_{2,0}}\varphi_\alpha$. Matrix A_1 is also diagonalizable with the following two eigenvalues:

$$\lambda_\pm = \bar{u} + \sqrt{C_{2,0}}\frac{1}{2}\left(q_1 \pm \sqrt{4+q_1^2}\right).$$

Neither of these eigenvalues is an eigenvalue of J. The eigenvalue

$$\lambda_{10} = \frac{\partial \overline{M}_{1,4}}{\partial M_{0,4}} = \bar{u} + \sqrt{C_{2,0}}\sum_{\alpha=1}^{4} w_\alpha \varphi_\alpha C_{2|\alpha}^2 \frac{\partial \eta^\star}{\partial C_{0,4}} = \bar{u} + \sqrt{C_{2,0}}\mathcal{K}_2,$$

where

$$\mathcal{K}_2 = \frac{\sum_{\alpha=1}^4 w_\alpha \varphi_\alpha \left(C_{2|\alpha}^\dagger\right)^2}{\sum_{\alpha=1}^4 w_\alpha (C_{2|\alpha}^\dagger)^2} = \frac{\sum_{\alpha=1}^4 w_\alpha \varphi_\alpha \left(b_0 + b_1\varphi_\alpha\right)^2}{\sum_{\alpha=1}^4 w_\alpha (b_0+b_1\varphi_\alpha)^2} = \frac{b_1(2b_0+b_1q_1)}{b_0^2+b_1^2},$$

is real and distinct.

It thus remains to show that the two eigenvalues of A_2 are real and distinct. The two eigenvalues of A_2 are

$$\lambda_\pm = \bar{u} - \frac{1}{2}\sqrt{C_{2,0}}\left[\varrho q_2 - \left(\frac{\partial \overline{C}_{1,3}}{\partial M_{0,3}}\right)^\dagger \pm \varrho\sqrt{\Delta}\right]$$

where $\Delta = [(a_{11}+a_{22})^2 - 4(a_{11}a_{22}-a_{12}a_{21})]/(\varrho^2 C_{2,0})$. Thus, a sufficient condition is that $\Delta > 0$ where

$$\Delta = \left[\frac{1}{\varrho}\left(\frac{\partial \overline{C}_{1,3}}{\partial M_{0,3}}\right)^\dagger + q_2\right]^2 + \frac{4}{\varrho}\left[3\bar{v}^\dagger\left(\frac{\partial \overline{C}_{1,3}}{\partial M_{0,3}}\right)^\dagger + \left(\frac{\partial \overline{C}_{1,3}}{\partial M_{0,2}}\right)^\dagger\right]. \tag{42}$$

It is straightforward to show that Δ does not depend on $\bar{v}^\dagger$ so that it can be evaluated at $\bar{v}^\dagger = 0$. Expanding $\Delta(\varrho, q_1, q_2, \eta_1)$ about $\varrho = 0$ yields

$$\Delta = 4(3+q_2^2) + 3q_1q_2(2+q_2^2)\varrho + \mathcal{O}(\varrho^2),$$

and thus $\Delta > 12$ for small $|\varrho|$. This concludes the proof.

For larger $|\varrho|$, the condition that $C_{2|\alpha}^\dagger = b_0 + b_1\varphi_\alpha > 0$, where

$$\varphi_1 = \frac{1}{2}\left(q_1 + \sqrt{4\eta_1 - 3q_1^2 + 4\sqrt{(\eta_1-q_1^2)(\eta_1-q_1^2-1)}}\right) > 0,$$
$$\varphi_4 = \frac{1}{2}\left(q_1 - \sqrt{4\eta_1 - 3q_1^2 + 4\sqrt{(\eta_1-q_1^2)(\eta_1-q_1^2-1)}}\right) < 0,$$

leads to two functions that must be positive:

$$g_1(\varrho, q_1, q_2, \eta_1) = 1 + \varrho q_2|\varphi_1| - \varrho^2\left(q_1|\varphi_1| + 1\right) > 0,$$
$$g_4(\varrho, q_1, q_2, \eta_1) = 1 - \varrho q_2|\varphi_4| + \varrho^2\left(q_1|\varphi_4| - 1\right) > 0.$$

For given values of (q_1, q_2, η_1), these functions provide bounds on ϱ: $\varrho_{min} < \varrho < \varrho_{max}$. From (42), $\Delta(\varrho, q_1, q_2, \eta_1)$ can be found explicitly using symbolic software. For $\varrho_{min} < \varrho < \varrho_{max}$ it can be shown that $\Delta > 12$ when $\eta_1 \geq 1 + q_1^2$. When a conditional variance $C_{2|1} = 0$ or $C_{2|4} = 0$, it is likely that $\Delta > 0$ for all realizable values of $|\varrho| \leq 1$ so the that the moment system in (40) remains at least weakly hyperbolic. The numerical examples in §6.1 support this conjecture.

5.3. Kinetic-based flux

The moment transport system (39) has the form

$$\partial_t \mathbf{M} + \partial_{\mathrm{x}} \cdot \mathbf{F}(\mathbf{M}) = \overline{\mathbf{A}}$$

with flux vector $\mathbf{F} = (\mathbf{F}_x, \mathbf{F}_y)^t$ for the 10-moment vector $\mathbf{M}$. In our numerical implementation, the components of the fluxes for moment $M_{i,j}$ are computed using a kinetic-based definition:

$$F_{x;i,j} = \int_{\mathbb{R}} \left(\int_0^\infty f(t,\mathrm{x},\mathrm{v}) u^{i+1} v^j \,\mathrm{d}u \right) \mathrm{d}v + \int_{\mathbb{R}} \left(\int_{-\infty}^0 f(t,\mathrm{x},\mathrm{v}) u^{i+1} v^j \,\mathrm{d}u \right) \mathrm{d}v, \tag{43}$$

$$F_{y;i,j} = \int_{\mathbb{R}} \left(\int_0^\infty f(t,\mathrm{x},\mathrm{v}) u^{i} v^{j+1} \,\mathrm{d}v \right) \mathrm{d}u + \int_{\mathbb{R}} \left(\int_{-\infty}^0 f(t,\mathrm{x},\mathrm{v}) u^{i} v^{j+1} \,\mathrm{d}v \right) \mathrm{d}u. \tag{44}$$

Thus, for the non-degenerate case, we follow the example in (20) and use the flux-based quadrature in (25):

$$F_{x;i,j} = M_{0,0} \sum_{\alpha=1}^{4} w_\alpha \left[\max(0,\lambda_\alpha)^{i+1} + \min(0,\lambda_\alpha)^{i+1} \right] \Theta_{u,\alpha}^j \tag{45}$$

where the u-conditioned jth-order moment of v is defined by

$$\Theta_{u,\alpha}^j := \sum_{\beta=1}^{3} \rho_{\alpha\beta} \left(\bar{v} + \bar{v}_\alpha + v_{\alpha\beta} \right)^j = \sum_{\beta=1}^{4} w_\beta^\star \left(\bar{v} + \bar{v}_\alpha + C_{2|\alpha}^{1/2} \varphi_\beta^\star \right)^j \tag{46}$$

with weights $w_\beta^\star$ and eigenvalues $\varphi_\beta^\star$ found from $(0, 1, q^\star, \eta^*)$ as in (21). This yields

$$\begin{aligned}
\Theta_{u,\alpha}^0 &= 1, \\
\Theta_{u,\alpha}^1 &= \bar{v} + \bar{v}_\alpha, \\
\Theta_{u,\alpha}^2 &= (\bar{v} + \bar{v}_\alpha)^2 + C_{2|\alpha}, \\
\Theta_{u,\alpha}^3 &= (\bar{v} + \bar{v}_\alpha)^3 + 3(\bar{v} + \bar{v}_\alpha) C_{2|\alpha} + q^\star C_{2|\alpha}^{3/2}, \\
\Theta_{u,\alpha}^4 &= (\bar{v} + \bar{v}_\alpha)^4 + 6(\bar{v} + \bar{v}_\alpha)^2 C_{2|\alpha} + 4(\bar{v} + \bar{v}_\alpha) q^\star C_{2|\alpha}^{3/2} + \eta^\star C_{2|\alpha}^2
\end{aligned} \tag{47}$$

where $\bar{v}_\alpha$, μ_α^2, $q^\star$, and $\eta^\star$ are found with the flux-based quadrature and a limiter on b_1 to ensure $b_0 + b_1 \varphi_\alpha \geq 0$ for $\alpha = 1, 4$. The eigenvalues λ_α and weights w_α in (45) are the same as in (20) (i.e., they are found using q_1 and η_1).

Likewise, for the flux in the y direction,

$$F_{y;i,j} = M_{0,0} \sum_{\alpha=1}^{4} w_\alpha \left[\max(0,\lambda_\alpha)^{i+1} + \min(0,\lambda_\alpha)^{i+1} \right] \Theta_{v,\alpha}^j \tag{48}$$

where the v-conditioned jth-order moments of u is defined by

$$\Theta_{v,\alpha}^j := \sum_{\beta=1}^{3} \rho_{\alpha\beta} \left(\bar{u} + \bar{u}_\alpha + u_{\alpha\beta} \right)^j = \sum_{\beta=1}^{4} w_\beta^\star \left(\bar{u} + \bar{u}_\alpha + C_{2|\alpha}^{1/2} \varphi_\beta^\star \right)^j. \tag{49}$$

The eigenvalues λ_α and weights w_α in (48) are defined as in (20), but found using q_2 and η_2. In other words, the parameters in (45) and (46) are found by conditioning on u, while those in (48) and (49) by conditioning on v.

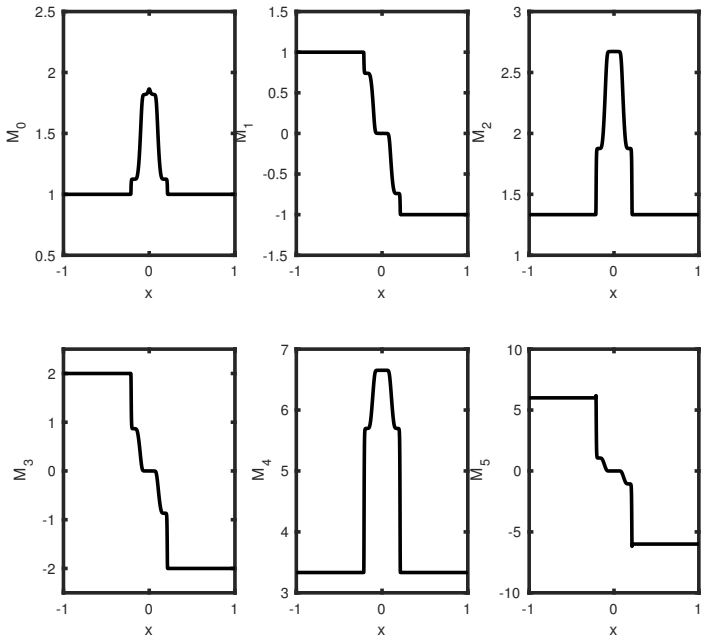

Figure 1: Solution to 1-D Riemann problem at $t = 0.1$. Five transported moments ($M_{0,\ldots,4}$) and reconstructed moment (M_5).

6. Numerical examples

As example applications, we consider a Riemann problem with 1-D velocity phase space, crossing jets in 2-D, and a Taylor–Green vortex problem with a 2-D velocity phase space. For each case, we solve the moment transport equations in (17) and (39), respectively.

6.1. 1-D Riemann problem

The initial conditions are defined on the real line with a step in the mean velocity at $x = 0$:

$$\bar{u} = \frac{M_1}{M_0} = \begin{cases} 1 & \text{if } x < 0, \\ -1 & \text{otherwise.} \end{cases}$$

For all x, the initial density is unity and the VDF is Maxwellian with energy $C_2 = 1/3$. The velocity distribution is assumed initially to be in equilibrium ($C_3 = 0$, $C_4 = 3C_2^2$). However, the discontinuous nature of the mean particle velocity quickly leads to particle trajectory crossing and a strongly non-equilibrium VDF.

In order to solve the moment equations numerically, the 1-D computational domain $-1 < x < 1$ is discretized into 2002 finite-volume cells. The spatial fluxes are treated using the first-order kinetic-based approach. The time step is chosen based on the largest magnitude of the abscissas u_α used to define the spatial fluxes with a CFL number of 0.5. Note that the maximum CFL number is determined from the largest eigenvalue of the spatial flux (e.g., (18) for three-node HyQMOM).

Simulation results for the 1-D Riemann problem are presented in Figs. 1–3 at time $t = 0.1$. We observe from Fig. 3 that the equilibrium condition is still present on the left and right sides of the computational domain. Note that unlike in a pure PTC problem where the velocity abscissas remain at their initial values,

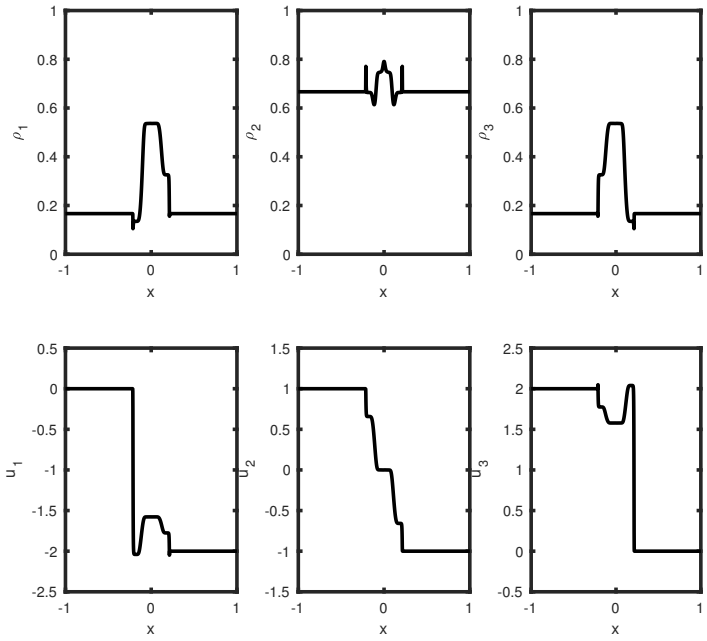

Figure 2: Solution to 1-D Riemann problem at $t = 0.1$. Top: quadrature weights $M_0\rho_\alpha$. Bottom: abscissas $\mathsf{u}_\alpha = \bar{u} + u_\alpha$.

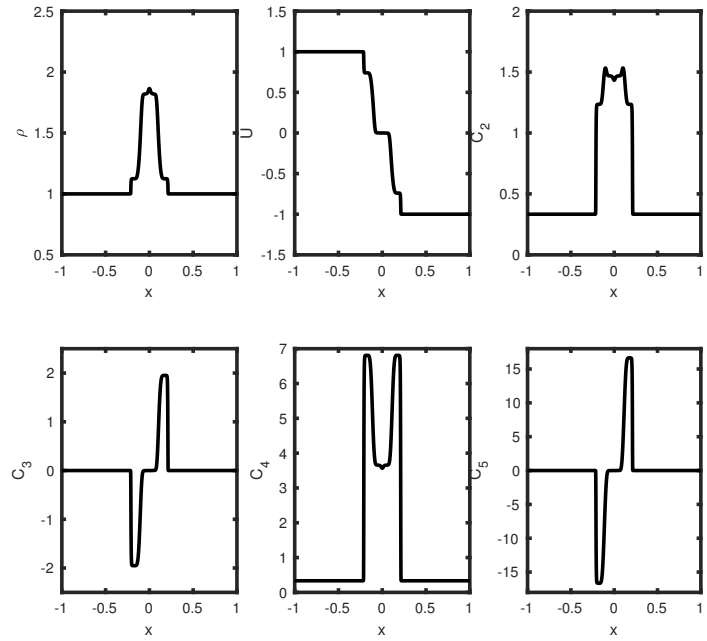

Figure 3: Solution to 1-D Riemann problem at $t = 0.1$. Top left: density M_0. Top center: mean velocity $\bar{u}$. Top right: C_2. Bottom left: C_3. Bottom center: C_4. Bottom right: C_5.

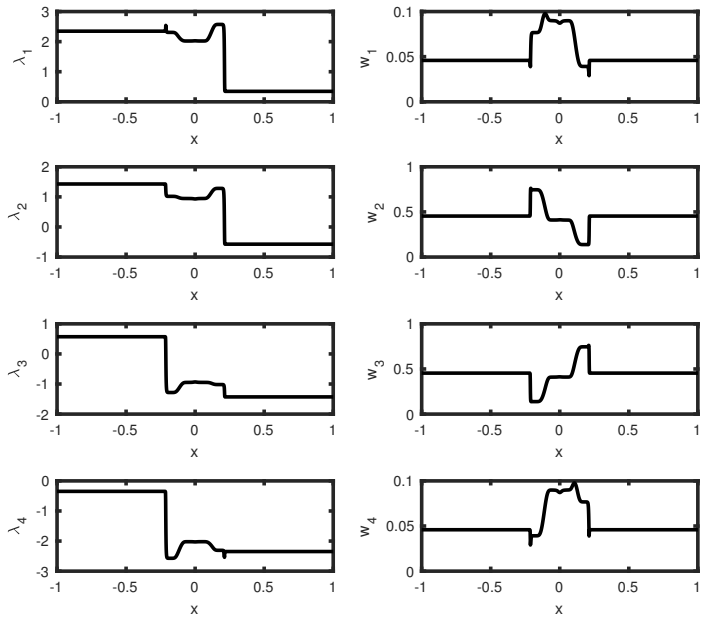

Figure 4: Solution to 1-D Riemann problem at $t = 0.1$. Flux-based quadrature in (20). Left: eigenvalues λ_α. Right: weights w_α. $\lambda_0 = \bar{u}$ and $w_0 = 0$ are not shown.

in Fig. 2 the abscissas have their largest magnitudes just behind the "shock" in density at the edge of the equilibrium domain. This behavior is a direct result of the definition of the spatial fluxes in terms of the underlying three-node HyQMOM distribution. Indeed, the outer tails of the Gaussian distribution have higher velocity than the value at the peak density and thus penetrate faster into the equilibrium domain, resulting in a higher local flux velocity. The strong deviations from equilibrium are also clearly observed in the central moments in Fig. 3.

Except at the edges of the equilibrium domain, we see from Fig. 1 that the transported moments are smoothly varying functions of x. More importantly, the singularities appearing in the solution do not belong to the class of δ-shocks but to the less singular class of shocks encountered with hyperbolic systems of conservation laws, thus revealing a potentially well-behaved system. Moreover, due to the eigenvalue-based definition of the spatial fluxes shown in Fig. 4, the moments are always realizable, and the moment-inversion algorithm always computes a well-defined quadrature from the updated moments. Overall, the three-node HyQMOM reconstruction of the velocity distribution yields a robust numerical algorithm using a minimum number of moments. In comparison to the high-order delta function reconstruction described in [17], the three-node HyQMOM provides a higher fidelity flux representation for a fixed number of transported moments. Moreover, because the moments of the HyQMOM distribution can be computed to any desired order, the flux representation described in §3.3 has the potential to be systematically improved. This advantage becomes even more significant for 2-D phase spaces where the number of transported moments needed for the delta-function reconstruction increases rapidly with the order of the moments [17].

6.2. 2-D crossing jets with compressive gas field

As in [18], CHyQMOM is applied here to simulate the crossings of two jets of particles in a compressible carrier phase by solving the ten-moment system in (39). The gaseous flow field is the following:

$$u_g(x, y) = u_{g,0}, \quad v_g(x, y) = \epsilon(y - 1) \tag{50}$$

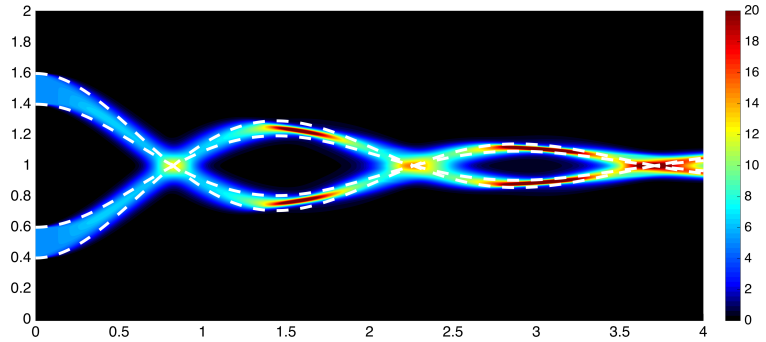

Figure 5: Number density in two-jet crossing with $\mathrm{St} = 20\mathrm{St}_c$ at steady state for CHyQMOM. White dashed lines represent the trajectories delineating the region where the particles lie in the analytical solution [18].

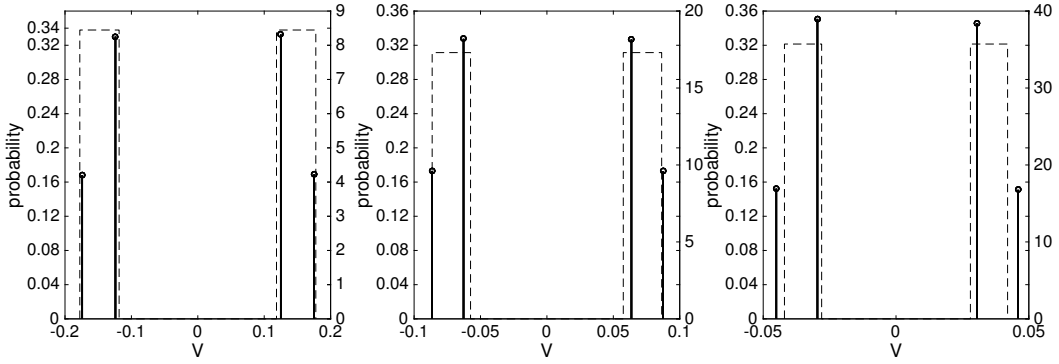

Figure 6: Probability density function for the vertical velocity at the three first crossing locations (from left to right) in two-jet crossing with $\mathrm{St} = 20\mathrm{St}_c$ at steady state for CHyQMOM (continuous black lines) and analytical solution (dashed lines).

and the acceleration terms are

$$\mathcal{A}_x = \frac{1}{\tau_p}(u - u_g), \quad \mathcal{A}_y = \frac{1}{\tau_p}(v - v_g)$$

where $u_{g,0} = 0.2\ \mathrm{m\,s^{-1}}$ is the axial gas velocity and $\epsilon = 1\ \mathrm{s^{-1}}$ is the rate of strain in the vertical direction. The dynamics of particles in this flow field are characterized by the Stokes number $\mathrm{St} = \epsilon\tau_p$, whose critical value $\mathrm{St}_c = 1/4$ delineates two regimes: for $\mathrm{St} < \mathrm{St}_c$, the particles are exponentially relaxing towards the centerline $y = 1\ m$, while for $\mathrm{St} > \mathrm{St}_c$ the particles will in addition oscillate around the centerline.

In Fig. 5, particles are injected with zero vertical velocity and the same axial velocity as the gas phase, through two slots at $x = 0$ and $y \in [0.4, 0.6]$ and $y \in [1.4, 1.6]$, and with a Stokes number $\mathrm{St} = 20\mathrm{St}_c$. Because of their high Stokes number and the symmetry of the injection around the centerline, the two jets cross each other at the centerline. It can be seen that CHyQMOM properly handles the particle trajectories as well as the crossing events. To further validate the ability of CHyQMOM to reproduce crossing events, the PDF of the vertical velocity component is presented in Fig. 6 at the three crossing locations. For CHyQMOM, these velocities correspond to the flux-based quadrature, i.e., to λ_α. It is worth mentioning that the analytical solution of the proposed configuration does not lead to a bidisperse velocity but to a double-window solution. Here we observe that the predicted velocities are close to the limits of the analytical solution.

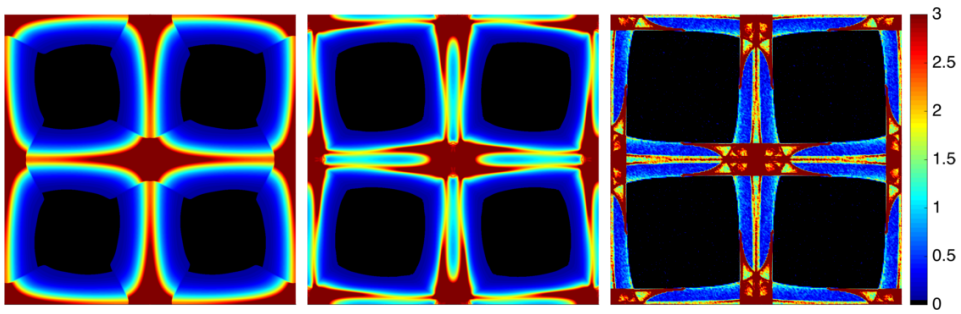

Figure 7: Number density in Taylor–Green vortices with $\mathrm{St} = 5\mathrm{St}_c$ at time $t = 2$ for AG (left), CHyQMOM (center) and Lagrangian (right) simulations.

6.3. 2-D Taylor–Green vortices

In this section, CHyQMOM is applied to simulate a 2-D Taylor–Green flow with Stokes drag [18] by solving the ten-moment system in (39). The gas-phase velocity components are

$$u_g(x, y) = \sin(2\pi x)\cos(2\pi y), \quad v_g(x, y) = -\cos(2\pi x)\sin(2\pi y);$$

and the acceleration terms are

$$\mathcal{A}_x = \frac{1}{\mathrm{St}}(u - u_g), \quad \mathcal{A}_y = \frac{1}{\mathrm{St}}(v - v_g).$$

With these definitions, the moment acceleration terms from (38) are closed. The moment system is solved on a unit-square domain with grid resolutions 256^2, 512^2 and 1024^2 to illustrate grid convergence. Unless stated otherwise, all results are shown for the 512^2 resolution. For comparison, a six-moment system (i.e., up to second order) with the anisotropic Gaussian (AG) closure [18] and a Lagrangian particle method are solved on the same grids. Details concerning the latter can be found in [18] where similar comparisons are made with a four-moment isotropic Gaussian (IG) closure. At time $t = 0$, the particles are uniformly distributed in the computational domain with zero velocity.

For 2-D Taylor–Green flow, there exists a critical Stokes number $\mathrm{St}_c = \frac{1}{8\pi}$ [18], below which the particle velocity variance is null (i.e., the central moments are null) and above which particle trajectory crossings (PTC) occur, making the particle velocity distribution multi-modal and the central moments non-null. When $\mathrm{St} = \mathrm{St}_c$, all particles accumulate at the edges of the vortices (see Fig. 9 in [18]). By its nature, the Lagrangian simulation can capture all PTC events and thus yields the highest fidelity solution. In contrast, the AG closure does not allow for PTC (which requires knowledge of the third-order moments), while the CHyQMOM closure can capture (locally) one PTC event. In any case, when the moment closures are unable to reproduce the multi-modal velocity distribution, the number density field $M_{0,0}$ is 'smoothed out' relative to the Lagrangian field.

In Figs. 7–9, number density fields at $t = 2$ are shown for the three methods at three different Stokes numbers: $5\mathrm{St}_c$, $10\mathrm{St}_c$ and $20\mathrm{St}_c$, respectively. In comparison to AG, the CHyQMOM result in Fig. 7 captures the primary PTC seen in the Lagrangian result for $\mathrm{St} = 5\mathrm{St}_c$. However, as expected, near the center of the domain where multiple PTC occur, the moment closures cannot capture the fine details present in the Lagrangian simulation. As the Stokes number increases, more and more PTC occur. For the largest Stokes number shown in Fig. 9, CHyQMOM captures more fine details as compared to AG, but both moment closures are significantly 'smoother' than the Lagrangian field.

As done in [18], the time-dependent behaviors of the three simulation methods are compared using the following statistics:

$$g_p = \frac{\{M_{0,0}^2\}}{\{M_{0,0}\}^2}, \quad \delta\tilde{\theta}_p = \frac{\{M_{0,0}(C_{2,0} + C_{0,2})\}}{2\{M_{0,0}\}}, \quad \tilde{E}_p = \frac{\{M_{2,0} + M_{0,2}\}}{2\{M_{0,0}\}}$$

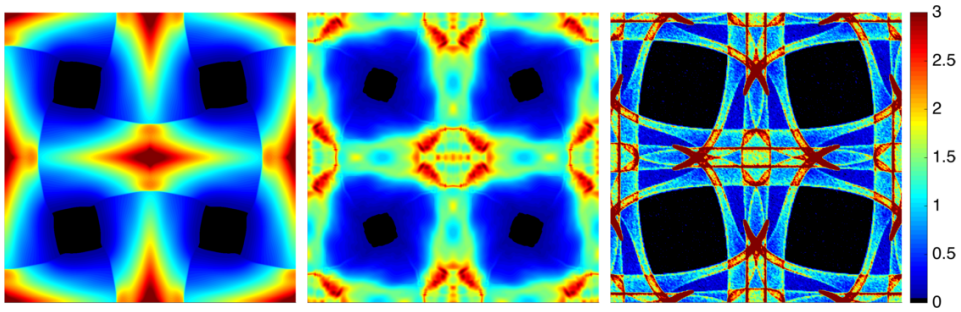

Figure 8: Number density in Taylor–Green vortices with $\mathrm{St} = 10\mathrm{St}_c$ at time $t = 2$ for AG (left), CHyQMOM (center) and Lagrangian (right) simulations.

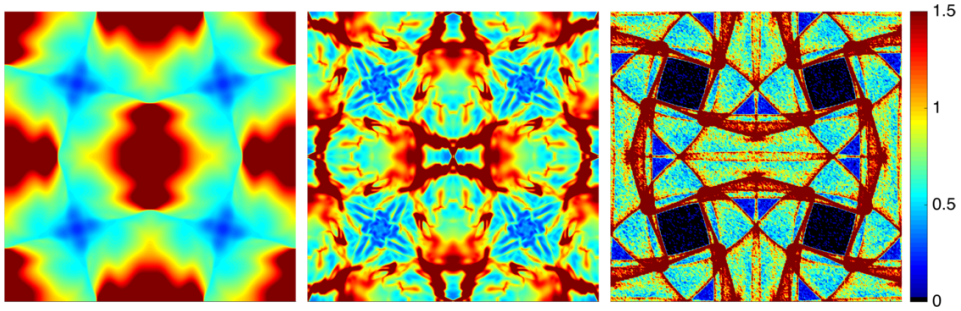

Figure 9: Number density in Taylor–Green vortices with $\mathrm{St} = 20\mathrm{St}_c$ at time $t = 2$ for AG (left), CHyQMOM (center) and Lagrangian (right) simulations.

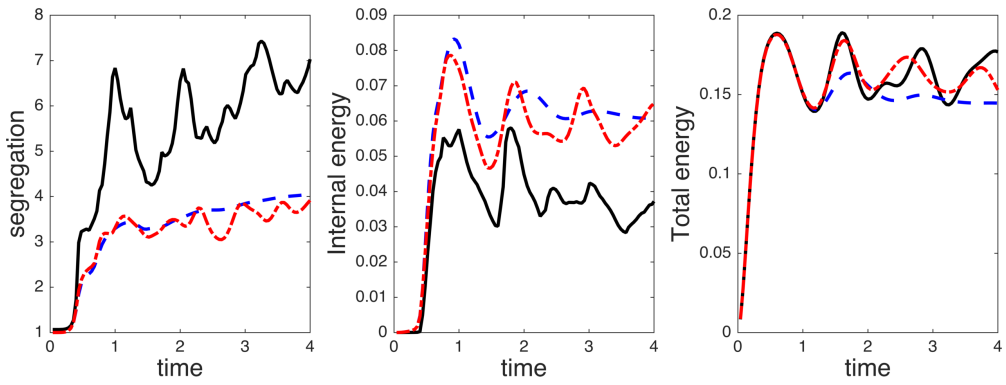

Figure 10: Time evolution of segregation, internal energy and total energy in Taylor–Green vortices with $\mathrm{St} = 5\mathrm{St}_c$ for AG (blue dashed line), CHyQMOM (red dot-dashed line) and Lagrangian (black line) simulations.

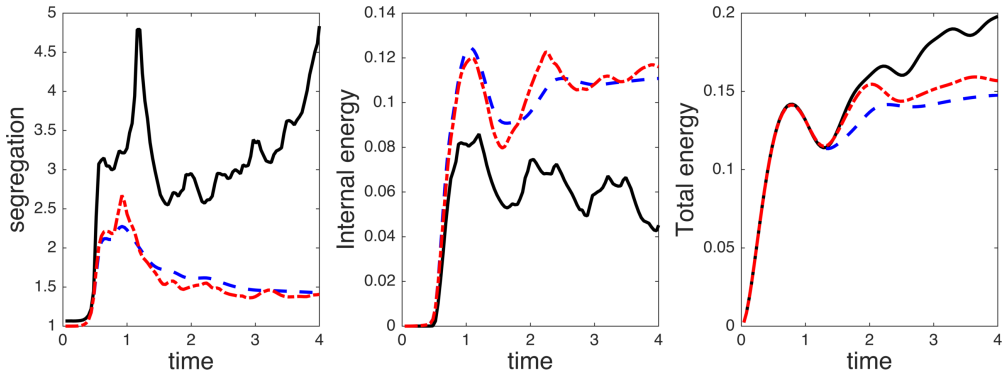

Figure 11: Time evolution of segregation, internal energy and total energy in Taylor–Green vortices with $\mathrm{St} = 10\mathrm{St}_c$ for AG (blue dashed line), CHyQMOM (red dot-dashed line) and Lagrangian (black line) simulations.

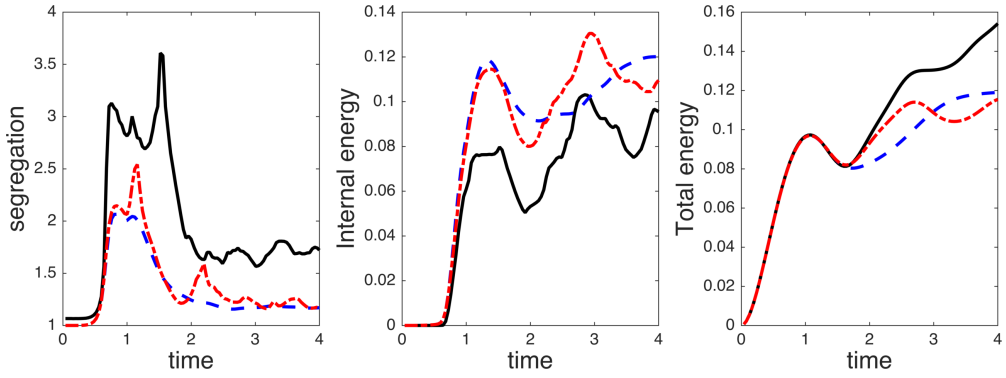

Figure 12: Time evolution of segregation, internal energy and total energy in Taylor–Green vortices with $\mathrm{St} = 20\mathrm{St}_c$ for AG (blue dashed line), CHyQMOM (red dot-dashed line) and Lagrangian (black line) simulations.

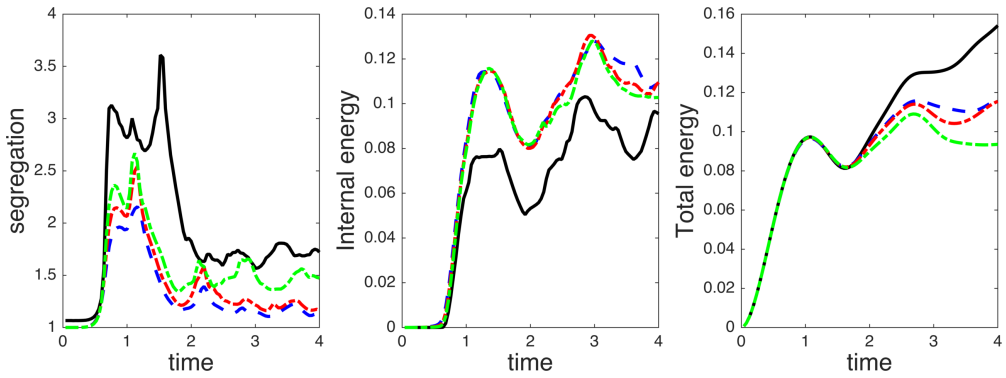

Figure 13: Time evolution of segregation, internal energy and total energy in Taylor–Green vortices with $\mathrm{St} = 20\mathrm{St}_c$ for Lagrangian (black line) and CHyQMOM with 256^2 (blue), 512^2 (red) and 1024^2(green) mesh cells.

where $\{\cdot\}$ denotes the spatial average over all grid cells. The segregation index g_p measures the degree of non-uniformity of the number density field. The internal energy $\delta\tilde{\theta}_p$ is a measure of the level of velocity fluctuations (i.e., the granular temperature or spatially uncorrelated kinetic energy [19, 20, 21]), while the total energy $\tilde{E}_p$ measure the total kinetic energy transferred from the fluid to the particle phase.

In Figs. 10–12, these statistics are plotted for each simulation method for the three Stokes numbers, respectively. Qualitatively, the statistics for the AG and CHyQMOM closures are very similar (especially when compared to IG statistics in [18]). This would imply that adding more moments by increasing N in CHyQMOM will lead to only a small improvement in the energy statistics as compared to the Lagrangian simulations. Overall, CHyQMOM does a better job than AG in capturing the time-dependence of the statistics, particularly for $t > 2$. However, the most obvious advantage of CHyQMOM with $N = 3$ over AG is its ability to capture PTC, and thus to provide a higher fidelity representation of the number density field in particle-laden flows with strong vorticity.

In Fig. 13, the dependence of the CHyQMOM statistics on the computational grid is shown for $\mathrm{St} = 20\mathrm{St}_c$. In general, for $t < 2.5$ the dependence on the grid is small. However, for larger times the segregation is higher for the finer grid. In contrast, the energy statistics are only weakly dependent on the grid resolution. We should emphasize that unlike with CQMOM [4], which is weakly hyperbolic [6], the hyperbolic nature of CHyQMOM should allow for grid-independent solutions on sufficiently fine grids with minimal additional computational cost. Indeed, with the modified CQMOM used in CHyQMOM, less moments are required with CHyQMOM as compared to the original 2-D CQMOM formulation in [4].

7. Conclusions

The conditional hyperbolic quadrature method of moments and the related moment-inversion algorithms introduced in this work appear to be a very promising approach for the direct-numerical simulation of the kinetic equation describing particle-laden turbulent flows [22, 23]. The proposed approach combines stability and a lower level of singularity compared to existing quadrature-based moment methods, see [6], and is able to capture both particle trajectory crossing (PTC) caused by the free-transport term and the effects of vortices. It is noteworthy that CHyQMOM naturally degenerates toward the correct velocity distribution with the associated spatial fluxes in both the PTC and dispersion limits. Moreover, by relying on the recent advances in CQMOM [4], the CHyQMOM naturally adapts to the required number of nodes in even highly degenerate cases (e.g., in the absence of particles). As such, the Eulerian moment methods described in this work should offer an attractive alternative to Lagrangian particle tracking methods for simulating particle-laden flows. Here, we have focused on HyQMOM with $N = 2$ and 3 nodes, but future work is warranted to determine the constraint on C_{2N-1} in HyQMOM needed to make the 1-D moment system hyperbolic for $N \geq 4$.

Acknowledgments

ROF was partially supported by grants from the U.S. National Science Foundation (CBET-1437865 and ACI-1440443).

Appendix A. Hankel matrices, moment space, and moment constraints

Let $\mathbf{M}$ be the vector of moments of a VDF $f(u)$ defined for $u \in \mathbb{R}$, and let C_j be the corresponding central moment of order j. The Hankel matrix $\mathbf{H}_n$ [13, 24], defined by

$$\mathbf{H}_n = \begin{bmatrix} C_0 & C_1 & \dots & C_n \\ C_1 & C_2 & \dots & C_{n+1} \\ \vdots & \vdots & \ddots & \vdots \\ C_n & C_{n+1} & \dots & C_{2n} \end{bmatrix}, \tag{A.1}$$

is non-negative if $|\mathbf{H}_n| \geq 0$. The moments $\mathbf{M}$ up to order $2n$ are realizable if $|\mathbf{H}_m|$ is non-negative for all $m \in \{0, 1, \dots, n\}$. The moments live in the interior of moment space if $|\mathbf{H}_m| > 0$ for all $m \in \{0, 1, \dots, n\}$, and reside on the boundary if $|\mathbf{H}_m| = 0$ for some $m \in \{0, 1, \dots, n\}$. Note that if $|\mathbf{H}_j| = 0$ then $|\mathbf{H}_m| = 0$ for $m > j$. In the main text, we make use of the conditions $|\mathbf{H}_1| = C_2 \geq 0$ and $|\mathbf{H}_2| = C_2C_4 - C_2^3 - C_3^2 \geq 0$ as the realizability conditions for the even-order moments for 2-node and 3-node HyQMOM, respectively. For infinite domains, the odd-order moments can take any value in $\mathbb{R}$.

The method for fixing C_{2N-1} in HyQMOM is related to the moment fluxes. In order for the Jacobian matrix of the 1-D moment fluxes for the moment system $\mathbf{M} = (M_0, \dots, M_{2N-2})^t$ to have an eigenvalue at $\bar{u}$, the following condition must hold for $N \geq 3$:

$$\left.\frac{\partial \overline{M}_{2N-1}}{\partial M_0}\right|_{M_1=0} = 0 \quad \Longrightarrow \quad 2N = 3 + \sum_{n=1}^{2N-4} n \frac{\partial \ln S_{2N-1}}{\partial \ln S_{n+2}} \tag{A.2}$$

where $S_n = C_n/C_2^{n/2}$ (e.g., $S_3 = q$ and $S_4 = \eta$) and S_{2N-1} depends only on $(S_3, \dots, S_{2N-2})$. We conjecture that (A.2) is satisfied when $|\bar{\mathbf{H}}^*_{N-1}| = 0$ where

$$\bar{\mathbf{H}}^*_{N-1} := \begin{bmatrix} 0 & 1 & S_3 & \dots & S_N \\ 1 & S_3 & S_4 & \dots & S_{N+1} \\ S_3 & S_4 & S_5 & \dots & S_{N+2} \\ \vdots & \vdots & \vdots & \ddots & \vdots \\ S_N & S_{N+1} & S_{N+2} & \dots & S_{2N-1} \end{bmatrix}. \tag{A.3}$$

For $N = 3$, $|\bar{\mathbf{H}}^*_2| = 0$ yields $S_5 = S_3(2S_4 - S_3^2)$. For $N = 4$, $|\bar{\mathbf{H}}^*_3| = 0$ yields

$$S_7 = \frac{2S_3^2S_4S_6 + S_3^2S_5^2 - 3S_3S_4^2S_5 - 2S_3S_5S_6 + S_4^4 - 2S_4^2S_6 + 2S_4S_5^2 + S_6^2}{S_5 - 2S_4S_3 + S_3^3}. \tag{A.4}$$

Both of these satisfy (A.2). Note, however, the S_7 is infinite for $S_5 = S_3(2S_4 - S_3^2)$, which is a realizable moment.

Using symbolic software, the seven eigenvalues of the moment system Jacobian found using (A.4) can be computed explicitly. Numerical tests reveal that the eigenvalues are real and distinct when the Hankel matrix $\mathbf{H}_3$ is positive. The eigenvalues are finite if $|\bar{\mathbf{H}}^*_2| \neq 0$, otherwise two eigenvalues are infinite and the remaining five correspond to those in the case $N = 2$. When the Hankel matrix $\mathbf{H}_3$ has zero determinant, but $\mathbf{H}_2$ is positive, two of the seven eigenvalues have multiplicity 2. Likewise when $|\mathbf{H}_2| = 0$, but $\mathbf{H}_1$ is positive, three of the seven eigenvalues have multiplicity 2. At present, it is unknown whether (A.4) is the unique choice, or, if not, whether a choice exists with finite eigenvalues for all realizable moment sets.

For $N = 5$, $|\bar{\mathbf{H}}_4^*| = 0$ yields a closure for S_9 that satisfies (A.2) and is finite for symmetric distributions. However, numerical tests show that some eigenvalues are complex for particular realizable moment sets. A general method is thus needed to determine C_{2N-1} for $N \geq 4$. As the N-node HyQMOM only requires that the moment set be realizable, and odd-order moments are not constrained, any method to choose C_{2N-1} that (i) is valid for all realizable moment sets up to C_{2N} and (ii) has $2N-1$ real eigenvalues for the moment system Jacobian could be used. An interesting observation from the cases with $N = 2$ and 3 is that the flux eigenvalues φ_α correspond to the Gauss–Hermite quadrature abscissas with 3 and 4 nodes, respectively, when the moments are Gaussian (i.e., $S_4 = 3$, $S_3 = S_5 = 0$). Continuing this pattern to $N = 4$ would require C_7 to be chosen such that the flux eigenvalues correspond to a 5-node Gauss–Hermite quadrature when $S_6 = 15$ and $S_7 = 0$. As there are seven φ_α for this case, the eigenvalue $\varphi_0 = 0$ would have a non-zero weight, and two others would have multiplicity two (e.g., $\varphi_1 = 2.85697$, $\varphi_2 = \varphi_3 = 1.35562$). The choice in (A.4) yields the 3-node, and not the 5-node, Gauss–Hermite quadrature with Gaussian moments.

Appendix B. 2-D, nine-node CHyQMOM with twelve moments

In this appendix, we briefly describe the extension of (24) using the symmetrical 12-moment set

$$\mathbf{M} = \begin{bmatrix} M_{0,0} & M_{0,1} & M_{0,2} & M_{0,3} & M_{0,4} \\ M_{1,0} & M_{1,1} & M_{1,2} & & \\ M_{2,0} & M_{2,1} & & & \\ M_{3,0} & & & & \\ M_{4,0} & & & & \end{bmatrix} \tag{B.1}$$

for the non-degenerate case. This moment set is of interest because all third-order moments (which control the energy flux) are included. At the same time, the degenerate cases with exactly one or two velocity abscissas needed to handle particle-trajectory crossing at arbitrary angles are allowed.

For the moments in (B.1), the correlation parameters $\bar{v}_\alpha = a_0 + a_1 u_\alpha + a_2 u_\alpha^2$ in (24) are defined to have the following properties:

$$\sum_{\alpha=1}^{3} \rho_\alpha \bar{v}_\alpha = C_{0,1} = 0, \quad \sum_{\alpha=1}^{3} \rho_\alpha u_\alpha \bar{v}_\alpha = C_{1,1}, \quad \sum_{\alpha=1}^{3} \rho_\alpha u_\alpha^2 \bar{v}_\alpha = C_{2,1}, \tag{B.2}$$

which yields a linear system for the coefficients $(a_0, a_1, a_2)^t$:

$$\begin{bmatrix} 1 & 0 & C_{2,0} \\ 0 & C_{2,0} & C_{3,0} \\ C_{2,0} & C_{3,0} & C_{4,0} \end{bmatrix} \begin{bmatrix} a_0 \\ a_1 \\ a_2 \end{bmatrix} = \begin{bmatrix} 0 \\ C_{1,1} \\ C_{2,1} \end{bmatrix}. \tag{B.3}$$

This system has a unique solution if the central moments $C_{i,0}$ are in the interior of moment space (i.e., the system is non-degenerate: $C_{2,0} > 0$ and $C_{2,0}C_{4,0} > C_{2,0}^3 + C_{3,0}^2$). In the degenerate case $C_{2,0} = 0$, $\bar{v}_\alpha = 0$; and when $C_{2,0} > 0$ but $C_{2,0}C_{4,0} = C_{2,0}^3 + C_{3,0}^2$, $\bar{v}_\alpha = \frac{C_{1,1}}{C_{2,0}} u_\alpha$. Note that these two cases correspond to $\rho_2 = 1$ and $\rho_2 = 0$, respectively.

The additional parameters $\{\rho_{\alpha\,1}, \rho_{\alpha\,2}, \rho_{\alpha\,3}, v_{\alpha\,1}, v_{\alpha\,2},\}$ are determined from the conditional moments $\{C_{0|\alpha}, C_{1|\alpha}, C_{2|\alpha}, C_{3|\alpha}, C_{4|\alpha}\}$ using the three-node HyQMOM in §2.3. As shown in the main text, $C_{0|\alpha} = 1$ and $C_{1|\alpha} = 0$. Thus we compute $C_{2|\alpha} = b_0 + b_1 u_\alpha$ from (29) using $\{C_{0,2}, C_{1,2}\}$. This yields

$$\begin{aligned} \sum_{\alpha=1}^{3} \rho_\alpha C_{2|\alpha} &= b_0 = C_{0,2} - \sum_{\alpha=1}^{3} \rho_\alpha \bar{v}_\alpha^2, \\ \sum_{\alpha=1}^{3} \rho_\alpha u_\alpha C_{2|\alpha} &= b_1 C_{2,0} = C_{1,2} - \sum_{\alpha=1}^{3} \rho_\alpha u_\alpha \bar{v}_\alpha^2. \end{aligned} \tag{B.4}$$

If one of the conditional variances is null, then b_1 is limited such that all conditional variances are non-negative

The conditional moments $C_{3|\alpha}$ and $C_{4|\alpha}$ are found from $\{C_{0,3}, C_{0,4}\}$ by assuming that they are depend on α through $C_{2|\alpha}$: $C_{3|\alpha} = q^\star C_{2|\alpha}^{3/2}$ and $C_{4|\alpha} = \eta^\star C_{2|\alpha}^2$. This yields

$$\begin{aligned} q^\star \sum_{\alpha=1}^{3} \rho_\alpha C_{2|\alpha}^{3/2} &= C_{0,3} - \sum_{\alpha=1}^{3} \rho_\alpha \bar{v}_\alpha^3 - 3 \sum_{\alpha=1}^{3} \rho_\alpha \bar{v}_\alpha C_{2|\alpha}, \\ \eta^\star \sum_{\alpha=1}^{3} \rho_\alpha C_{2|\alpha}^{2} &= C_{0,4} - \sum_{\alpha=1}^{3} \rho_\alpha \bar{v}_\alpha^4 - 6 \sum_{\alpha=1}^{3} \rho_\alpha \bar{v}_\alpha^2 C_{2|\alpha} - 4q^\star \sum_{\alpha=1}^{3} \rho_\alpha \bar{v}_\alpha C_{2|\alpha}^{3/2}, \end{aligned} \tag{B.5}$$

which are solved for $q^\star$ and $\eta^\star$. The realizability of $C_{4|\alpha}$ requires that $\eta^\star \geq 1 + (q^\star)^2$. If this condition is not met, then $q^\star$ and $\eta^\star$ are projected to the realizability curve $\eta^\star = 1 + (q^\star)^2$ in the direction of the Gaussian moments (i.e., $q^\star = 0$ and $\eta^\star = 3$). Three-node HyQMOM can then be applied for each α to find the remaining parameters.

Bibliography

[1] O. Desjardins, R. O. Fox, P. Villedieu, A quadrature-based moment method for dilute fluid-particle flows, J. Comput. Phys. 227 (4) (2008) 2514–2539.

[2] R. O. Fox, A quadrature-based third-order moment method for dilute gas-particle flow, J. Comput. Phys. 227 (12) (2008) 6313–6350.

[3] R. O. Fox, Higher-order quadrature-based moment methods for kinetic equations, J. Comput. Phys. 228 (2009) 7771–7791.

[4] C. Yuan, R. O. Fox, Conditional quadrature method of moments for kinetic equations, J. Comput. Phys. 230 (22) (2011) 8216–8246.

[5] F. Bouchut, S. Jin, X. Li, Numerical approximations of pressureless and isothermal gas dynamics, SIAM J. Numer. Anal. 41 (1) (2003) 135–158.

[6] C. Chalons, D. Kah, M. Massot, Beyond pressureless gas dynamics: quadrature-based velocity moment models, Commun. Math. Sci. 10 (4) (2012) 1241–1272.

[7] V. Vikas, Z. J. Wang, A. Passalacqua, R. O. Fox, Realizable high-order finite-volume schemes for quadrature-based moment methods, J. Comput. Phys. 230 (13) (2011) 5328–5352.

[8] C. Chalons, R. O. Fox, M. Massot, A multi-Gaussian quadrature method of moments for gas-particle flows in a LES framework, in: Proceedings of the Summer Program 2010, Center for Turbulence Research, Stanford University, Stanford, USA, 2010, pp. 347–358.

[9] M. Junk, Domain of definition of Levermore's five-moment system, J. Stat. Phys. 93 (5/6) (1998) 1143–1167.

[10] C. D. Levermore, W. J. Morokoff, The Gaussian moment closure for gas dynamics, SIAM J. Appl. Math. 59 (1996) 72–96.

[11] C. D. Levermore, Moment closure hierarchies for kinetic theories, J. Stat. Phys. 83 (1996) 1021–1065.

[12] C. Yuan, F. Laurent, R. O. Fox, An extended quadrature method of moments for population balance equations, J. Aerosol Sci. 51 (2012) 1–23.

[13] W. Gautschi, Orthogonal Polynomials: Computation and Approximation, Oxford University Press, Oxford, UK, 2004.

[14] B. Perthame, Kinetic formulation of conservation laws, Vol. 21 of Oxford Lecture Series in Mathematics and its Applications, Oxford University Press, Oxford, UK, 2002.

[15] D. L. Wright, Numerical advection of moments of the particule size distribution in Eulerian models, J. Aerosol Sci. 38 (3) (2007) 352–369.

[16] L. Fialkow, S. Petrovic, A moment matrix approach to multivariate cubature, Integr. Equ. Oper. Theory 52 (1) (2005) 85–124.

[17] R. O. Fox, Optimal moment sets for multivariate direct quadrature methods of moments, Indust. & Engng. Chem. Res. 48 (2009) 9686–9696.

[18] A. Vié, F. Doisneau, M. Massot, On the anisotropic Gaussian velocity closure for inertial-particle laden flows, Commun. Comput. Phys. 17 (01) (2015) 1–46.

[19] P. Février, O. Simonin, K. D. Squires, Partitioning of particle velocities in gas–solid turbulent flow into a continuous field and a spatially uncorrelated random distribution: theoretical formalism and numerical study, J. Fluid Mech. 533 (2005) 1–46.

[20] R. O. Fox, On multiphase turbulence models for collisional fluid–particle flows, J. Fluid Mech. 742 (2014) 368–424.

[21] J. Capecelatro, O. Desjardins, R. O. Fox, On fluid–particle dynamics in fully developed cluster-induced turbulence, J. Fluid Mech. 780 (2015) 578–635.

[22] S. Balachandar, J. K. Eaton, Turbulent dispersed multiphase flow, Annu. Rev. Fluid Mech. 42 (2010) 111–133.

[23] R. O. Fox, Large-eddy-simulation tools for multiphase flows, Annu. Rev. Fluid Mech. 44 (2012) 47–76.

[24] H. Dette, W. J. Studden, The Theory of Canonical Moments with Applications in Statistics, Probability, and Analysis, Wiley Series in Probability and Statistics: Applied Probability and Statistics, John Wiley & Sons Inc., New York, 1997.